UW MET No.81.05.H1

Case Studies
Employing Satellite Indirect Soundings

Department of Meteorology
University of Wisconsin–Madison
1225 W. Dayton Street
Madison, Wisconsin 53706

Contributions by

A. G. Blechman
L. H. Horn
T. L. Koehler
B. A. Paulson

L. H. Horn, Principal Investigator

FINAL REPORT

The research in this report has been supported
by the National Environmental Satellite Service of the
National Oceanic and Atmospheric Administration under Grant 04-4-158-2

May 1981

Case Studies
Employing Satellite Indirect Soundings

Department of Meteorology
University of Wisconsin–Madison
1225 W. Dayton Street
Madison, Wisconsin 53706

Contributions by

A. G. Blechman
L. H. Horn
T. L. Koehler
B. A. Paulson

L. H. Horn, Principal Investigator

FINAL REPORT

The research in this report has been supported
by the National Environmental Satellite Service of the
National Oceanic and Atmospheric Administration under Grant 04-4-158-2

May 1981

TABLE OF CONTENTS

INTRODUCTION

This report serves as the Final Report for research supported by the National Oceanic and Atmospheric Administration under Grant 04-4-158-2 (Case Studies Employing Satellite Indirect Soundings). Previous work under this grant was presented in two project reports, Meteorological Applications of Satellite Indirect Soundings, August 1977, and Meteorological Applications of Satellite Indirect Soundings II, December 1977. The fundamental goal of this grant has been to seek methods which facilitate the application of satellite indirect soundings to significant meteorological problems, especially by field forecasters. In addition, some effort has been devoted to developing various objective techniques which enhance the application of satellite sounding data.

Many of our satellite sounding studies have focused on upper tropospheric wind maxima (jets). Our reasons for this emphasis has been two-fold: 1) the most active weather situations are associated with propagating jet maxima and 2) although lacking good vertical resolutions, satellite soundings are capable in describing thermal gradients in the deep layer below the jet streak. The article by Blechman and Horn represents an initial attempt at using finer resolution satellite soundings to better monitor propagating jet streaks in the upper troposphere. Previous studies using satellite soundings to locate jet maxima have employed operational soundings. Blechman and Horn show that reducing the number of individual soundings combined to yield an operational sounding, can improve the meteorologist's ability to locate and monitor jet streaks.

Paulson an Horn more closely examine the possiblity of using even finer resolution soundings. They examined and edited individual Nimbus-6 soundings (i.e., single scan spot observations) using an interactive video-graphic system. Various data sets were obtained which demonstrate the effect of different types of averaging. They note that soundings derived from individual scan spots provide only minor improvements over DST soundings based on averages of up to 84 single soundings. However, a data set derived from averages of five individual soundings was distinctly superior to the DST data set in defining 850, 500 and 300 mb temperature fields, 850-300 mb thickness fields and 500 mb height fields. Results from their various experiments indicate that 500 mb height fields calculated from these 5 scan

spot averages are comparable to 500 mb height fields derived from only mandatory level radiosonde temperatures.

The article by Koehler evaluates several methods that can be used to interpolate data from nonuniformly spaced satellite sounding locations to an evenly spaced grid. An absolute measure of interpolation accuracy was provided by using analytic fields to define the data values at both the nonuniform observation points and at grid points. Koehler found two methods superior in this satellite sounding example. Of these two, optimum interpolation is preferred because it proved less expensive. However, prior screening of satellite data for obviously poor soundings is still necessary before constructing grid point analyses from them.

Lyle H. Horn
Principal Investigator
May 1981

THE INFLUENCE OF HIGHER RESOLUTION NIMBUS-6 SOUNDINGS IN LOCATING JET MAXIMA

BY

Amy Gene Blechman and Lyle H. Horn

University of Wisconsin-Madison

Abstract

The retrieval of vertical temperature profiles (i.e., satellite soundings) from satellite measured radiances offers the meteorologist a vast new array of data which have the potential of improving weather forecasts. These new data may eventually improve weather prediction by providing the truly global coverage needed for large-scale numerical prediction models and, also by providing the field forecaster with upper air data possessing greater spatial and temporal resolution than is available in the current radiosonde data. This improved resolution can assist the forecaster in monitoring especially active weather situations. One such application - locating and tracking of jet streaks - is examined in this paper. The jet streak feature is especially well suited for description using satellite soundings since it can be identified by the strong and deep baroclinic zone beneath it. Because of the large depth of the baroclinic zone, the well known lack of vertical resolution in satellite soundings is largely overcome in such a study.

Previous studies from Nimbus-5 and -6 have successfully described jet streaks using operational soundings commonly consisting of averages of up to 84 individual soundings. (These are the Data Systems Test, DST, soundings.) This paper goes a step further by examining the results achieved from higher horizontal resolution Nimbus-6 soundings which are based on a maximum of 28 spot soundings, and referred to as the 4 x 7 soundings.

A 25 August 1975 case was selected for this study since there was an unusually strong jet streak over the United States and attendant severe weather. Two cross sections through the jet core were used to make comparisons of the effectiveness of the higher resolution soundings and the coarser DST soundings in describing the jet core speed, latitude and altitude. The 4 x 7 and DST results are verified against the corresponding radiosonde data using an isentropic cross section approach. In both cross sections, the higher resolution data gave distinctly better speed, latitude and altitude descriptions of the jet streak.

1. Introduction

The retrieval of vertical temperature and moisture profiles from satellites represents a milestone for atmospheric observations. Satellite soundings should eventually lead to improved forecasts, first by providing numerical models with a truly global set of observations and second, by furnishing field forecasters with more frequent and closer spaced soundings than the conventional 0000 and 1200 GMT radiosonde observations. This paper focuses on the second point.

Several previous studies have demonstrated that satellite soundings which are carefully screened of poor data can adequately describe synoptic features that are of concern to the field forecaster. For example, Petersen and Horn (1977) used Nimbus-6 soundings to track a closed 500 mb low. Of more potential importance to the forecaster is the ability of the satellite temperature soundings to define the hyperbaroclinic zone beneath upper tropospheric wind maxima. Many major, often rapidly changing, weather events are associated with these jet phenomena. Togstad and Horn (1974), using simulated data found that thermal gradients derived from satellite soundings could define the location and intensity of the polar jet. In subsequent work Kapela and Horn (1975) and Horn et al., (1976) used thermal gradients derived from Nimbus-5 and Nimbus-6 soundings to describe especially strong upper tropospheric jets.

In this paper Nimbus-6 soundings from one orbital pass over the United States were used in an attempt to describe the thermal support of a jet streak. This study differs from previous ones because higher resolution satellite sounding data are used in different combinations in an attempt to produce a data set which is superior to the lower resolution Data Systems Test (DST) soundings used in most earlier studies. Before describing the basic data sets in detail the experiment, the general characteristics of jet streaks and their significance to the field forecaster will be briefly examined in the next section.

2. Jet streaks, severe weather and satellite soundings

The most active weather areas are commonly associated with propagating jet maxima which Palmén and Newton (1969) have labeled jet streaks. Within the jet stream, jet streaks are areas of stronger winds with weaker jet stream winds found upstream and downstream. The maximum winds typically range from 50-70 m s^{-1}.

Jet streaks, usually relatively long narrow features, are associated with short waves in the upper troposphere. Typically they propagate eastward with or slightly faster than the upper level wave. Since the air within the jet streak travels at a much faster speed (e.g., 60 m s^{-1}) than the jet streak propagation speed (e.g., 20 m s^{-1}), air enters the west or rear of the jet streak called the entrance region and leaves at the east or forward edge called the exit region. In passing through the jet streak the air parcel experiences a positive acceleration on entering, and a negative acceleration on exiting. This leads to a transverse component to the upper tropospheric flow in both the entrance and exit regions - toward lower isobaric contours in the entrance region and toward higher contours in the exit region. A direct transverse circulation exists in the entrance region and on indirect circulation in the exit region. The vertical stretching associated with the indirect circulation in the right front quadrant of the jet streak leads to weaker static stability. Sechrist and Johnson (1970) have referred to this as dynamic destabilization. In a study of the 300 mb jet on Colorado cyclogenetic days Hovanec and Horn (1975), Achtor and Horn (1981) and Marshment and Horn (1981) have corroborated this region of weaker static stability. In another study Uccellini and Johnson (1979) have simulated the destabilization process using a hybrid isentropic-sigma coordinate numerical model.

Figure 1a shows the 300 mb jet and a static stability field at 1200 GMT on 3 April 1974, preceding the great tornado outbreak that occurred later that day. In this figure the static stability is presented in the form of the pressure increment (Δp_θ) between the 310 and 315 K isentropic surface. Large values of Δp_θ indicate weak stability. Figure 1b also shows the 1200 GMT 300 mb jet, the 1200 GMT surface fronts and the severe weather outlook issued by the National Weather Service earlier that morning. (Of the 148 tornadoes on April 3, 140 occurred within the outlook area.) The positions of three powerful squall lines which developed on the afternoon of 3 April are shown. Certainly, the position of the jet maxima was significant to the location of the severe weather. While Fig. 1 deals with only a single case, albeit a critical one, Fig. 2 from Hovanec and Horn (1975) represents a composite showing the mean 300 mb isotachs and a modified Showalter index field for 39 cases of spring season Colorado cyclogenesis. The significantly weaker static stability in the right front quadrant of the jet is clearly evident.

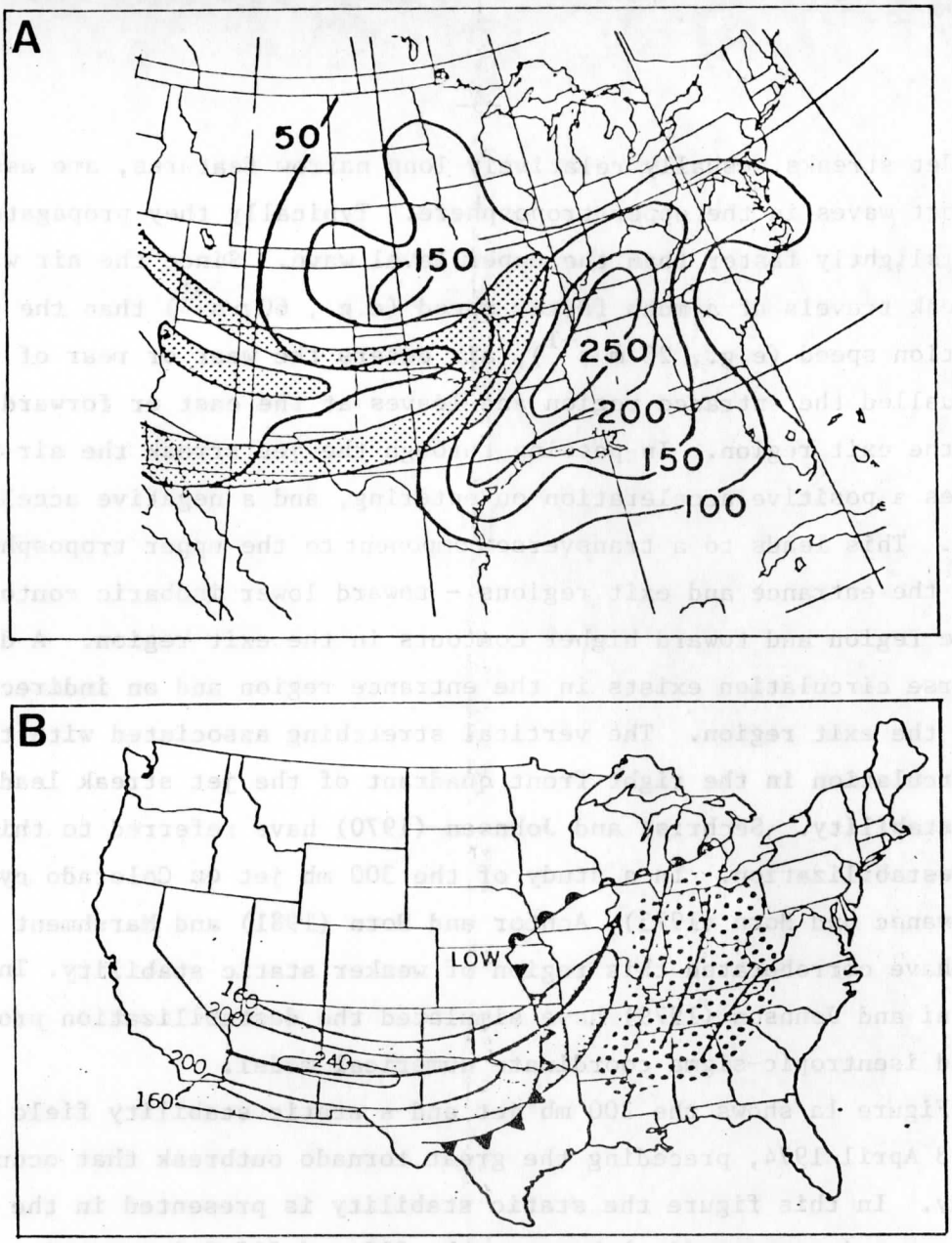

Figure 1. The relationship between the jet core and the static stability field at 1200 GMT 3 April 1974 using ΔP_θ between the 310 and 315 K isentropic surfaces. Isotachs at 300 mb are stippled in alternating 10 m s^{-1} intervals with a maximum of 65 m s^{-1}. (B) Depiction of fronts and jet (km hr^{-1}) at 1200 GMT. The stippled area outlines the severe weather outlook area issued by the National Weather Service, while the dark lines show the location of three powerful squall lines at 2035 GMT. (From Trewartha and Horn, 1980.)

Most severe thunderstorms and tornadoes commence after local noon (1800 GMT in the Central Time Zone) and often continue until local midnight (See Fig. 3.). Under the current radiosonde schedule, upper level data for the crucial period between 1800 GMT and about 0200 GMT consists of observations which are between six and fourteen hours old (0000 GMT data are not available to the forecaster until 0200 GMT). Thus, the time gap in radiosonde observations combined with the narrowness of a jet streak, make monitoring it a formidable task.

Satellite soundings can be of special value in tracking this feature. Although the satellite soundings lack the vertical resolution of radiosonde soundings, the thermal support for a jet streak represents the vertically integrated thermal (or thickness) gradient through a deep layer of the troposphere. Thus the lack of vertical detail in the satellite data does not present a formidable problem in locating jet maxima. Furthermore, the fairly dense horizontal array of satellite soundings can assist the forecaster in locating jet streaks which may slip between radiosonde stations which often have greater spacings than the satellite data even over the United States.

In monitoring jet streaks a geostationary satellite capable of providing soundings throughout the day would be ideal. This capability should become an operational reality when the VISSR Atmospheric Sounder (VAS) type soundings become available on a routine basis over the central United States. The soundings, along with wind observations obtained from satellite cloud trackings, can provide the valuable additional data needed for mesoscale or subsynoptic models. Certainly, important features for inclusion in these models are the location, propagation and intensity of jet streaks. Contributions to this future effort in forecast improvement can be made now by seeking methods which optimally employ satellite soundings to locate propagating jet maxima. Fortuitously, the polar orbiting Nimbus-6 satellite, while in full operation, passed over the central United States near midday local time - a time close to the onset of severe weather. It provided temperature profiles necessary to define the thermal support for the jet. The sensor instrument packages, particularly the infrared sounder aboard Nimbus-6 are basically the same as those aboard TIROS-N and NOAA-6. Consequently, the general results obtained here regarding the influence of higher resolution soundings can be applied to other satellites.

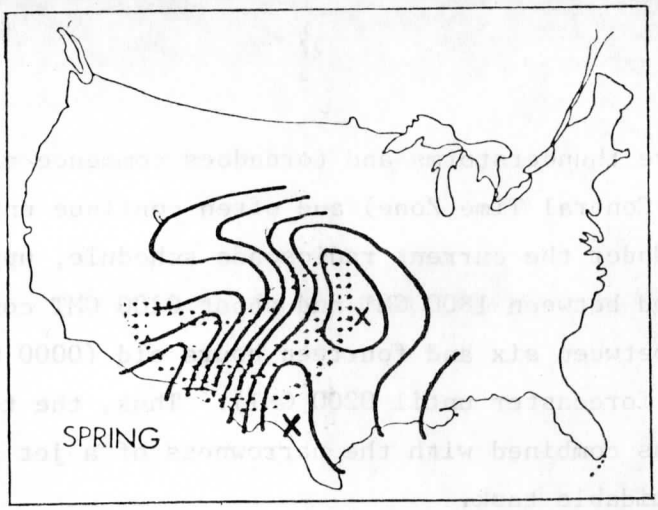

Figure 2. Mean 300 mb isotachs for the developing spring cases on days of cyclogenesis (alternating intervals are shaded in 2.5 m s^{-1} increments from a central core of 40 m s^{-1}) superimposed on the modified Showalter index field (solid lines are 1°C increments from the 7°C minima marked with X). (Figure adapted from Hovanec and Horn, 1975.)

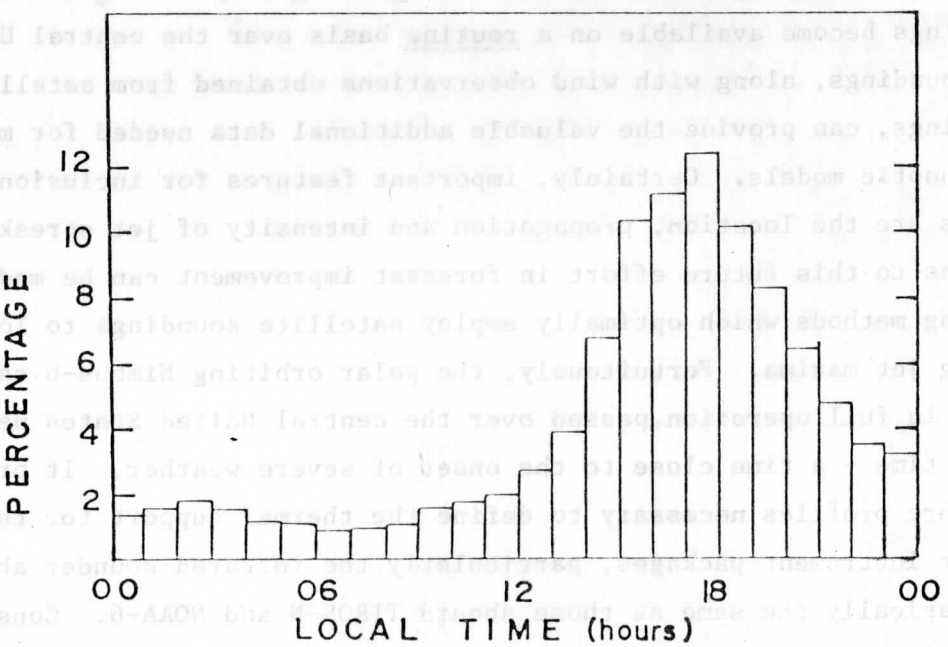

Figure 3. Percentage of tornadoes at given times of day. (After Winston, 1956)

3. The Nimbus-6 system

As noted previously, the major goal of this paper is to determine if Nimbus-6 data combined to form higher resolution soundings can provide an improved description of the thermal field beneath jet streaks.

a) The instrument

Nimbus-6 was launched on 12 June 1975 in a 1100 km sun-synchronous polar orbit. Each orbit required 107.25 minutes and 26.8° separated successive equatorial crossings. The orbit of Nimbus-6 passed over the Midwest near 0600 and 1800 GMT. Vertical temperature profiles were obtained from radiances measured by two instruments aboard the satellite: the High-resolution Infra-red Sounder (HIRS) and the Scanning Microwave Spectrometer (SCAMS). These instruments scanned about 700 km to the right and left of the orbital track. HIRS detected radiation in two portions of the infrared spectrum in the 15 μm and 4.3 μm CO_2 bands. The 15 μm band (channels 1-7) and the 4.3 μm band (channels 11-16) were complementary in temperature sensitivity. The 15 μm band was more sensitive to temperatures of relatively cold regions, while the 4.3 μm band was more sensitive to temperatures of the relatively warmer troposphere. Microwave measurements were made by SCAMS in five channels: three of them near the 5 mm wavelength were used to determine temperature profiles. It is important to note these microwave channels were not significantly influenced by non-precipitating clouds. See the Nimbus-6 User Guide (NASA, 1975) for more detail.

b) Radiance processing

As Nimbus-6 moved along its orbital path, the HIRS instrument scanned from left to right making 42 spot observations during each scan line. Periodic instrument calibration during the scanning process resulted in gaps in the radiance data. Twenty scans were made between these gaps, thus producing a total of 840 fields of view (42 fields of view per each of 20 scan lines). A single field of view directly below the orbital path consisted of a 29 km diameter circle at the earth's surface. Ideally, 840 soundings, each roughly 30 km apart could be obtained between calibrations. The density of this enormous amount of data was about 85 times that of the conventional United States radiosonde network in the contiguous forty-eight states.

However several factors, including clouds, varying surface emissivities and instrument noise, produced individual radiances unsuited for temperature

retrievals. Also, the high data density of soundings at 30 km intervals was impractical and unmanageable for most purposes. The National Environmental Satellite Service, NESS, divided the 840 member array into thirty subsets of twenty-eight individual HIRS fields of view. The subsets were called HIRS 4 x 7 blocks because each contained four fields of view along the orbital path by seven fields of view across the orbital path (See Fig. 4.). Within a 4 x 7 block, HIRS measurements were checked for consistency against SCAMS measurements interpolated to the HIRS field of view. When differences exceeded certain predetermined acceptance criteria (which varied by season) that field of view was ignored. Radiances in the remaining fields of view were combined in a manner described by Smith and Woolf (1976). This method which was designed to minimize the effect of cloud contamination, yielded a set of "clear-column" (cloud-free) infrared radiances representative of the 4 x 7 blocks with locations shown by X's in Figure 4. These cloud-free infrared radiances were supplemented with SCAMS microwave radiances interpolated to the cloud-free radiance locations. If the number of HIRS fields of view which failed the initial gross consistency checks became too large within a 4 x 7 block, no cloud-free radiances were derived for that block. The cloud-free infrared and microwave radiances available at the X locations in Figure 4 were of the proper form for input into the temperature retrieval techniques.

c) The DST soundings

NESS initially supplied temperature profiles for each acceptable 4 x 7 location. However, the National Meteorological Center (NMC) found that even this number of soundings within the prescribed area was overwhelming. Consequently, a maximum of twelve rather than thirty soundings was chosen as a manageable number for the global data sets being generated. This reduction was made by averaging up to three sets of cloud-free 4 x 7 radiances. Temperature retrievals were then made at these locations using the eigenvector approach described in Smith and Woolf (1976). These retrievals are the so-called "DST soundings" which have been used in most studies. Because there were only five 4 x 7 cloud-free radiances along the orbital path between calibration intervals, overlapping averaging was required to obtain the DST soundings. Examples of this averaging process are shown in Figure 4. For instance, on the far left side of the diagram (column A) cloud-free radiances (X's) in blocks 1, 2 and 3 were averaged to yield the DST sounding indicated by a square (□) centered in block 2 and blocks 3, 4 and 5 were used to obtain a second sounding

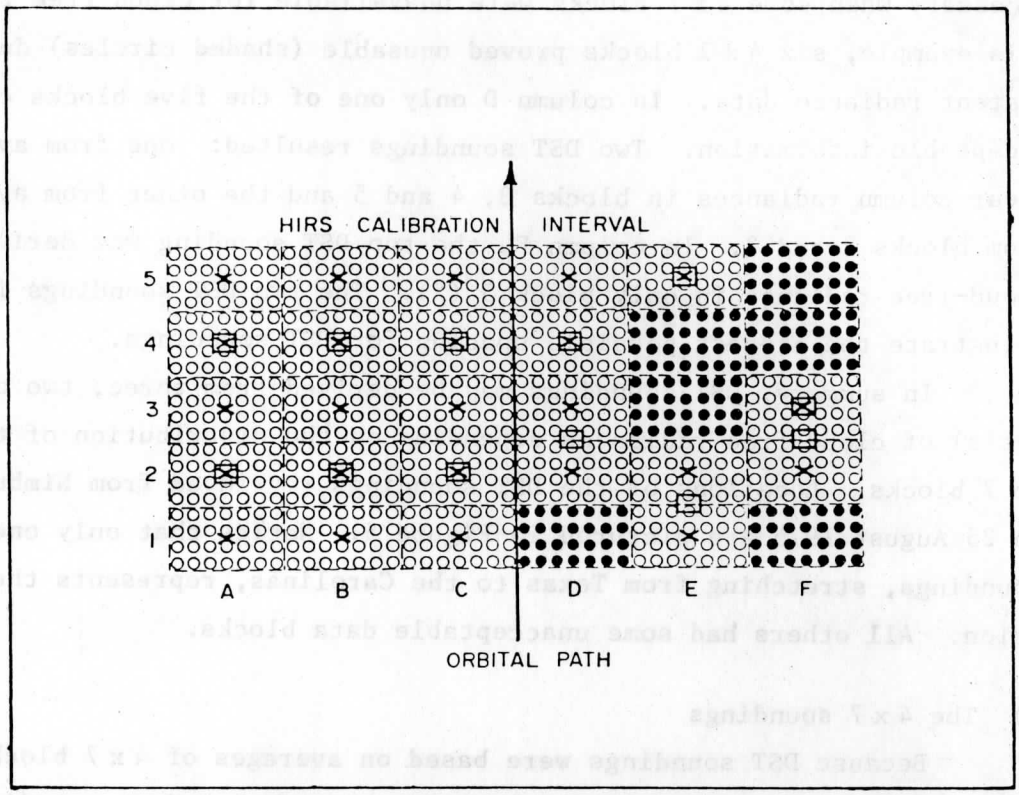

Figure 4. Schematic of a Nimbus-6 scan between calibration intervals to illustrate the HIRS data averaging process. The dashed lines enclose HIRS 4x7 blocks. Circles represent individual HIRS fields of view. An X stands for the composite 4x7 sounding in each block. The DST soundings are represented by ☐'s. For illustrative purposes, the unshaded circles are acceptable HIRS data and the shaded circles unacceptable. Therefore, blocks filled with shaded circles represent areas where there are an inadequate number of acceptable HIRS measurements to permit a sounding retrieval within that block. (See text.)

centered on block 4.

Examples to the right of the orbital track show the averaging that was necessary when some 4 x 7 blocks were unavailable for cloud-free radiances. In this example, six 4 x 7 blocks proved unusable (shaded circles) due to inconsistent radiance data. In column D only one of the five blocks contained unacceptable information. Two DST soundings resulted: one from averaging clear-column radiances in blocks 3, 4 and 5 and the other from averaging data from blocks 2 and 3. In column E, the top DST sounding was derived from the cloud-free radiance in only block 5 (X). The two DST soundings in column F illustrate the closest possible spacing for DST soundings.

In summary, DST soundings may be derived from three, two or even one set(s) of cloud-free radiances depending on the distribution of the unusable 4 x 7 blocks. Locations of the DST soundings retrieved from Nimbus-6 radiances on 25 August 1975 are pictured in Figure 5. Notice that only one group of DST soundings, stretching from Texas to the Carolinas, represents the ideal situation. All others had some unacceptable data blocks.

d) The 4 x 7 soundings

Because DST soundings were based on averages of 4 x 7 blocks of HIRS radiance data, it was decided to examine the results from soundings based on single 4 x 7 blocks. Unfortunately, it was impossible to obtain the individual 4 x 7 cloud-free radiances used in the DST soundings. Rather, the National Environmental Satellite Service reprocessed the original radiance data. Again cloud-free radiances were obtained and an eigenvector approach employed to produce soundings based on individual 4 x 7 blocks of radiance data. However, less stringent acceptance criteria were used for this reprocessing, yielding more 4 x 7 blocks than the DST processing. This is illustrated in Figure 6 which shows the positions of 4 x 7 soundings. Note that in Iowa, Minnesota and North Dakota, the reprocessed soundings would produce more DST soundings than those obtained during the Data Systems Test (Fig. 5). Additionally, some of the soundings would have slightly different locations as a comparison of Figures 5 and 6 shows.

4. The data sets and experiment

The previous section indicates that a great deal of horizontal averaging is done to obtain a single DST sounding. As noted in the introduction, satellite soundings lack the vertical resolution of radiosonde observations,

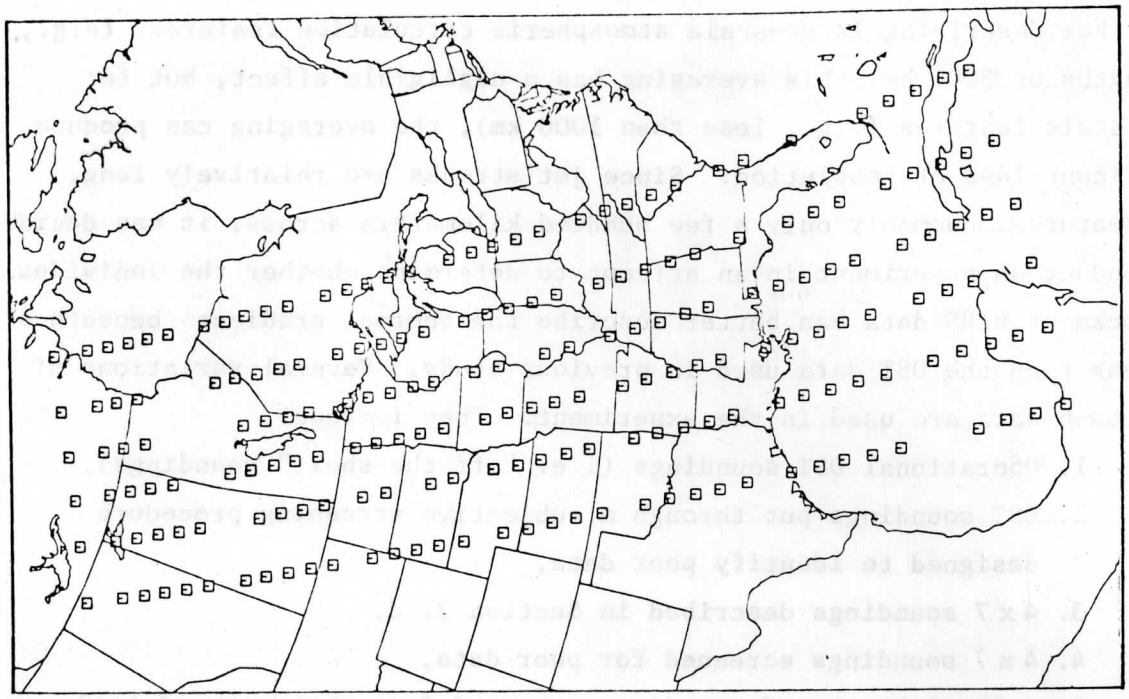

Figure 6. The 4x7 sounding locations at 1715 GMT 25 August 1975.

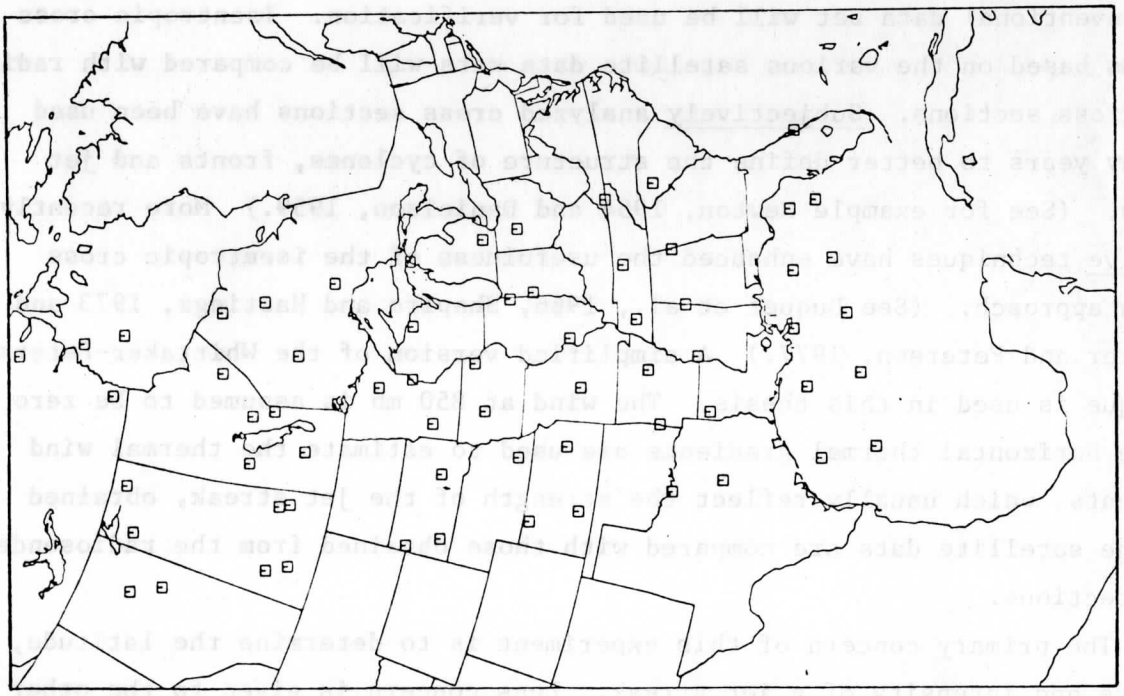

Figure 5. The DST sounding locations at 1715 GMT 25 August 1975.

but offer the possibility of excellent horizontal resolution. However, the averaging which is done to obtain DST soundings reduces the horizontal resolution. For describing large-scale atmospheric circulation features, (e.g., wave lengths of 3000 km) this averaging has a negligible effect, but for smaller scale features (e.g., less than 1000 km), the averaging can produce a significant loss of resolution. Since jet streaks are relatively long, narrow features, commonly only a few hundred kilometers across, it was decided to conduct an experiment in an attempt to determine whether the individual 4 x 7 blocks of HIRS data can better describe the thermal gradients beneath a jet streak than the DST data used in previous study. Several variations of the Nimbus-6 data are used in the experiment. They include:

1. Operational DST soundings (i.e. "off the shelf" soundings),
2. DST soundings put through a subjective screening procedure designed to identify poor data,
3. 4 x 7 soundings described in Section 3, d,
4. 4 x 7 soundings screened for poor data,
5. A DST-like set of soundings composed from the screened 4 x 7 soundings.

Although it is recognized that radiosonde data are not error-free, this conventional data set will be used for verification. Isentropic cross sections based on the various satellite data sets will be compared with radiosonde cross sections. Subjectively analyzed cross sections have been used for many years to better define the structure of cyclones, fronts and jet streaks. (See for example Newton, 1954 and Danielson, 1959.) More recently, objective techniques have enhanced the usefulness of the isentropic cross section approach. (See Duquet et al., 1966, Shapiro and Hastings, 1973 and Whittaker and Petersen, 1977.) A simplified version of the Whittaker-Petersen technique is used in this thesis. The wind at 850 mb is assumed to be zero and the horizontal thermal gradients are used to estimate the thermal wind components, which usually reflect the strength of the jet streak, obtained from the satellite data are compared with those obtained from the radiosonde cross sections.

The primary concern of this experiment is to determine the latitude, altitude and intensity of a jet streak. Less concern is given to the other features of the wind field since it is the core of the jet streak that is related to severe weather outbreaks.

5. The synoptic case and procedures

The first step towards testing and applying Nimbus-6 satellite soundings was finding a day with a strong jet maximum and severe weather. The choice was limited because Nimbus-6 data were not available prior to July 1975 and in early September 1975 the 15 μm channels became noisy. This eliminated a case study during the spring season when major severe weather outbreaks are more common. In spite of the brief operational period a case meeting the criteria was found. This was 25-26 August 1975.

The surface and upper air synoptic conditions on 25-26 August 1975 are pictured in Figure 7. At 1200 GMT 25 August, a 1020 mb high in the Carolinas dominated the southeastern United States. A cold front trailed from an unusually deep (980 mb) low northeast of Lake Winnipeg through northwest Wisconsin across Iowa and Kansas (Fig. 7a). The 500 mb low with central height of 5430m was practically vertical with the surface system. A trough extended into the north central states. Superimposed on the 500 mb height field of Figure 7b are 300 mb isotachs. They reveal a jet located from the northwest coast of Washington extending southeastward to Wyoming then curving northeastward through Minnesota. The strongest winds (i.e. the jet streak) were located from South Dakota into Minnesota. This 50 m s^{-1} core is strong for summer.

By 1800 GMT (Fig. 7c) the southeast high had moved off the east coast and the Canadian low reached a central pressure of 976 mb. Meanwhile, the cold front pushed into Missouri and Texas. At 0000 GMT showed the low had moved northeastward into Hudson Bay and slightly weakened (Fig. 7d). At this time, the cold front edged into northern lower Michigan and trailed across the central part of the nation. At 0000 GMT the 300 mb jet was a bit broader and slightly farther south with a 50 m s^{-1} core (Fig. 7e). The major weather with this system was a series of slow-moving squall lines in Missouri from which copious rains fell, including the heaviest report of 219.61 mm in 24 hours at Shell City.

Two cross sections based on Nimbus-6 data were selected which were approximately perpendicular to the core of the 300 mb jet. The locations of the cross sections are shown in Figure 8 for the DST data, Figure 9 for the 4 x 7 data and Figure 10 for the radiosonde data. The radiosonde cross sections were chosen as close to parallel to the satellite cross sections as possible. The cross sections are most clearly described in terms of the

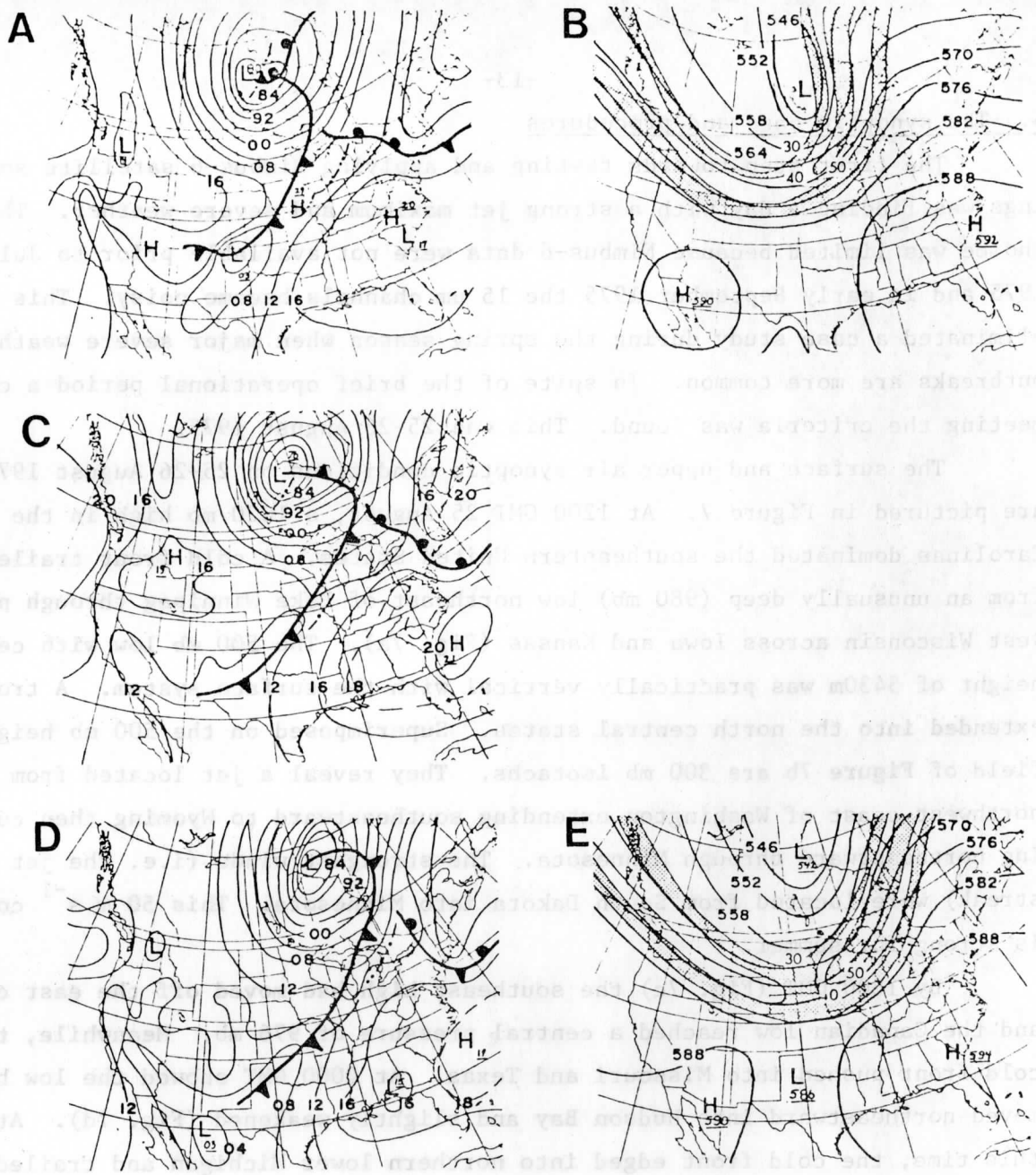

Figure 7. (A) Surface analysis for 1200 GMT 25 August 1975. (B) 500 mb height analysis with superimposed 300 mb isotachs in 10 m s^{-1} intervals for 1200 GMT 25 August 1975. (C) Same as (A) except 1800 GMT. (D) Same as (A) except 0000 GMT 26 August. (E) Same as (B) except 0000 GMT 26 August 1975.

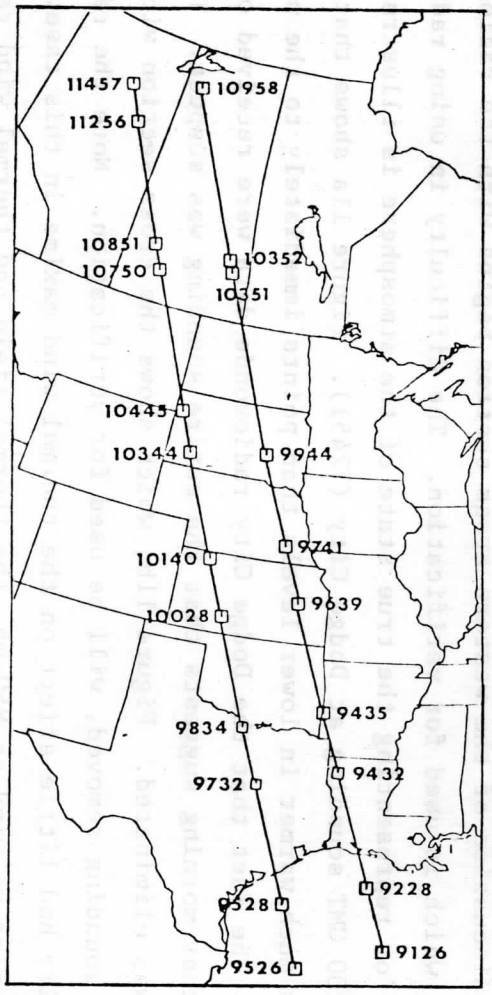

Figure 8. Locations of the DST cross sections.

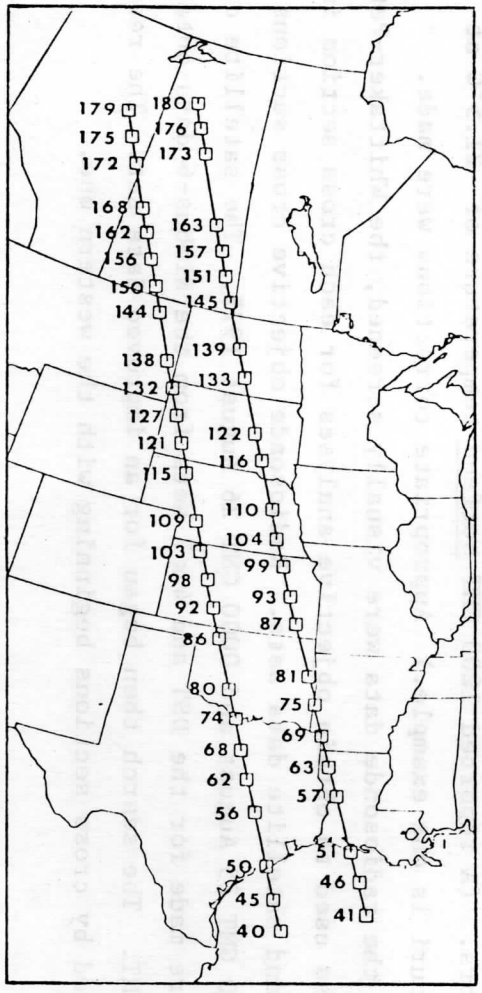

Figure 9. Locations of the 4x7 cross sections.

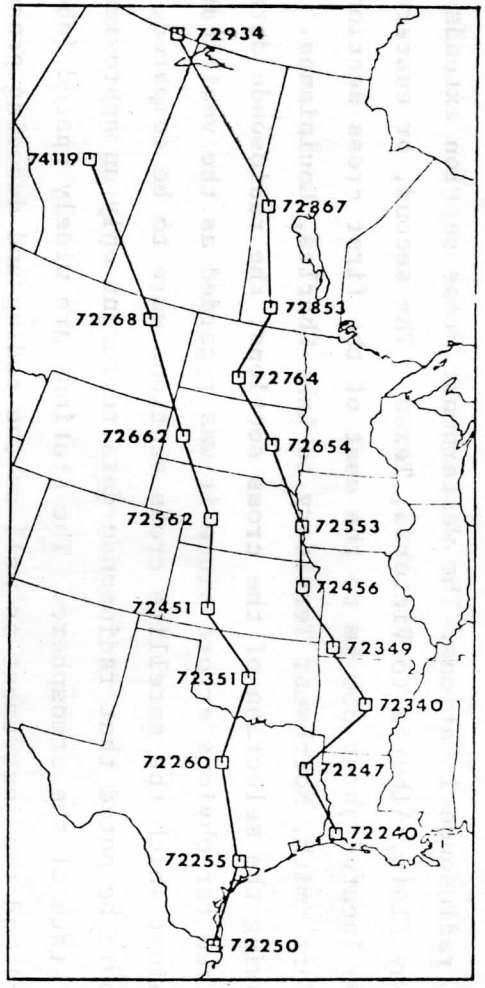

Figure 10. Locations of the radiosonde cross sections.

conventional radiosonde locations. The westernmost cross section extends from Edmonton Stony Plain, Alberta to Victoria, Texas. The second, or eastern cross section located about 350 km to the east of the first cross section extends from Fort Smith, Northwest Territory to Lake Charles, Louisianna.

Following the selection of the cross sections, the radiosonde data set was scrutinized for obvious errors since it was regarded as the verification standard against which the satellite cross sections were to be compared. However, it should be noted that radiosonde data represent only an approximation of the true state of the atmosphere. The stations are widely spaced (about 400 km apart) and the instrument as well as the coding and decoding procedures are susceptible to error. This first screening was accomplished by plotting suspect soundings on a Stüve thermodynamic diagram and by visually spotting obvious errors. (A reported 1200 GMT surface temperature of -21.5°C at Monet, Missouri is one example.) Appropriate corrections were made.

Once the radiosonde data were visually screened, the Whittaker-Petersen technique was used to obtain objective analyses for each cross section in the radiosonde and satellite data sets. Radiosonde objective cross sections were run for 1200 GMT 25 August and 0000 GMT 26 August 1975. The satellite cross sections were made for the DST and 4 x 7 sets from the Nimbus-6 data obtained near 1715 GMT. The search then began for an improved data set. The results are discussed by cross sections beginning with the western one.

6. Results

a) Western cross section

The discussion of the western cross section begins with the radiosonde description which is used for verification. The difficulty in using radiosonde data for representing the true state of the atmosphere is illustrated with the 1200 GMT sounding at Dodge City (72451). Figure 11a shows that this sounding is much warmer in lower levels than points immediately to the north and south. The fact that the Dodge City radiosonde data were received only to 400 mb that morning suggests that the entire sounding was suspect. Thus, the point was eliminated. Figure 11b, which shows the cross section with the Dodge City sounding removed, will be used for verification. Note the removal of Dodge City had little affect on the thermal wind maxima in this case.

Assuming no wind at 850 mb, the thermal field and thermal wind relationship produce a 60 m s^{-1} wind maximum at 42.3° north latitude and 250 mb

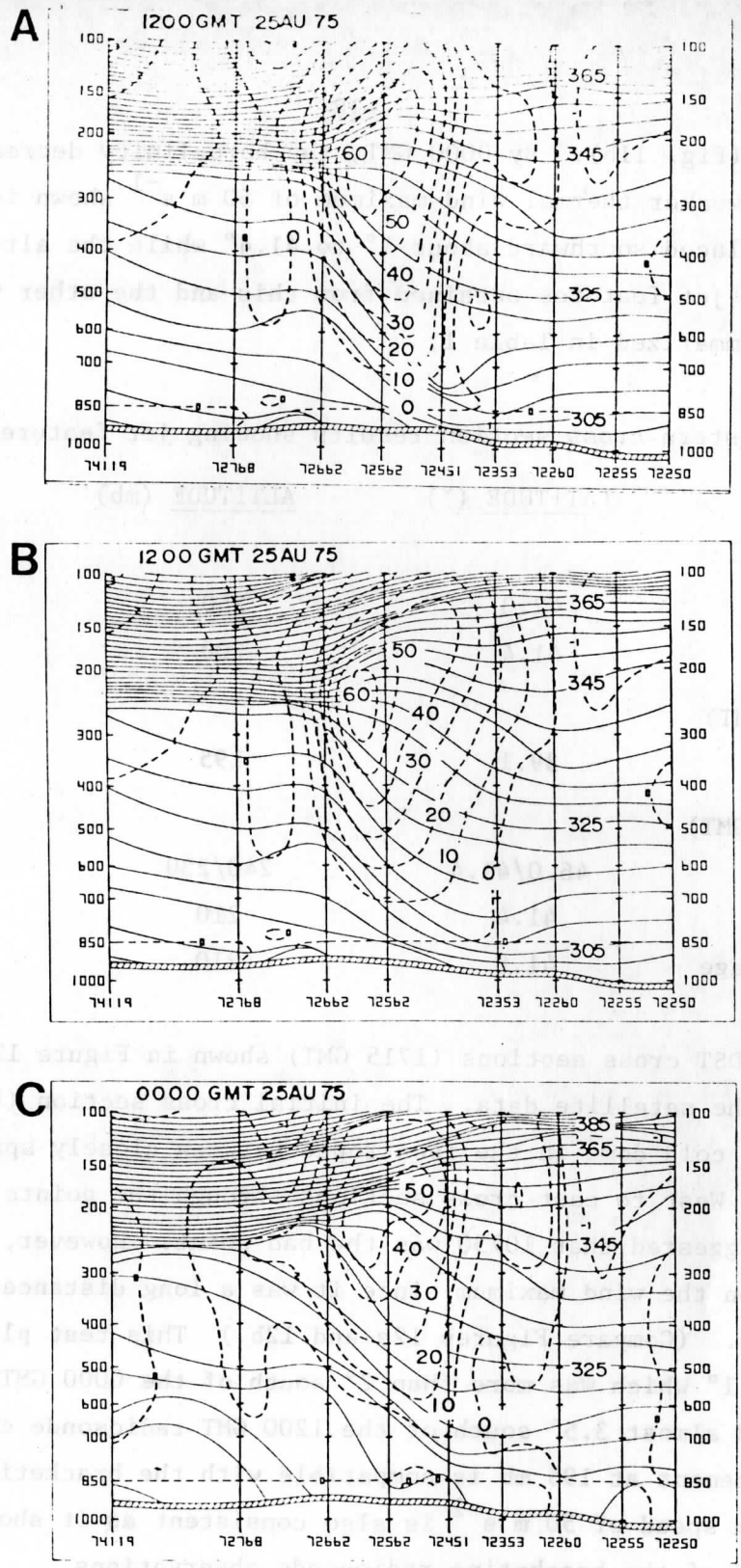

Figure 11. Western radiosonde cross section.
(A) 1200 GMT 25 August 1975 original.
(B) 1200 GMT 25 August 1975 corrected.
(C) 0000 GMT 26 August 1975.
Isotachs in m s^{-1} (dashed lines) and θ in K (solid lines).

at 1200 GMT (Fig. 11b). By 0000 GMT, the baroclinity decreased producing the broader and weaker thermal wind maximum of 50 m s^{-1} shown in Figure 11c. The core is displaced southward about 1° to 41.4° while the altitude increased to 200 mb. The jet features obtained from this and the other western cross sections are summarized in Table 1.

Table 1. Western cross section results showing jet features.

TEST	LATITUDE (°)	ALTITUDE (mb)	SPEED (m s^{-1})
RADIOSONDE			
1200 GMT	42.3	250	60
0000 GMT	41.4	200	50
DST (1715 GMT)			
Original	39.1	195	50
4 x 7 (1715 GMT)			
Original	46.0/41.4	240/230	30/50
Screened	41.4	210	50
DST Average	41.8	210	50

The DST cross sections (1715 GMT) shown in Figure 12 provide the first tests for the satellite data. The initial cross section (Fig. 12a) showed an apparent cold dome in the isentropes between closely spaced points 10851 and 10750. West to east cross sections through the points in question strongly suggested that 10750 was the bad point. However, its removal had no effect on the wind maximum since it was a long distance from the baroclinic zone. (Compare Figures 12a and 12b.) This test placed the central core at 39.1° which was more than 2° south of the 0000 GMT radiosonde cross section and almost 3.5° south of the 1200 GMT radiosonde cross section. Altitude placement at 195 mb is compatible with the bracketing radiosondes. The maximum speed of 50 m s^{-1} is also consistent as it shows the decreasing speed trend of the bracketing radiosonde observations.

The original 4 x 7 data shown in Figure 13a illustrates the noise accompanying higher resolution data. There are numerous ripples in the isentropes. The initial run produced a 50 m s^{-1} core at 41.4° with a weaker 20 m s^{-1} core at 46.0°. This pattern is inconsistent with the radiosonde data so the area was examined in some detail. Various procedures can be used

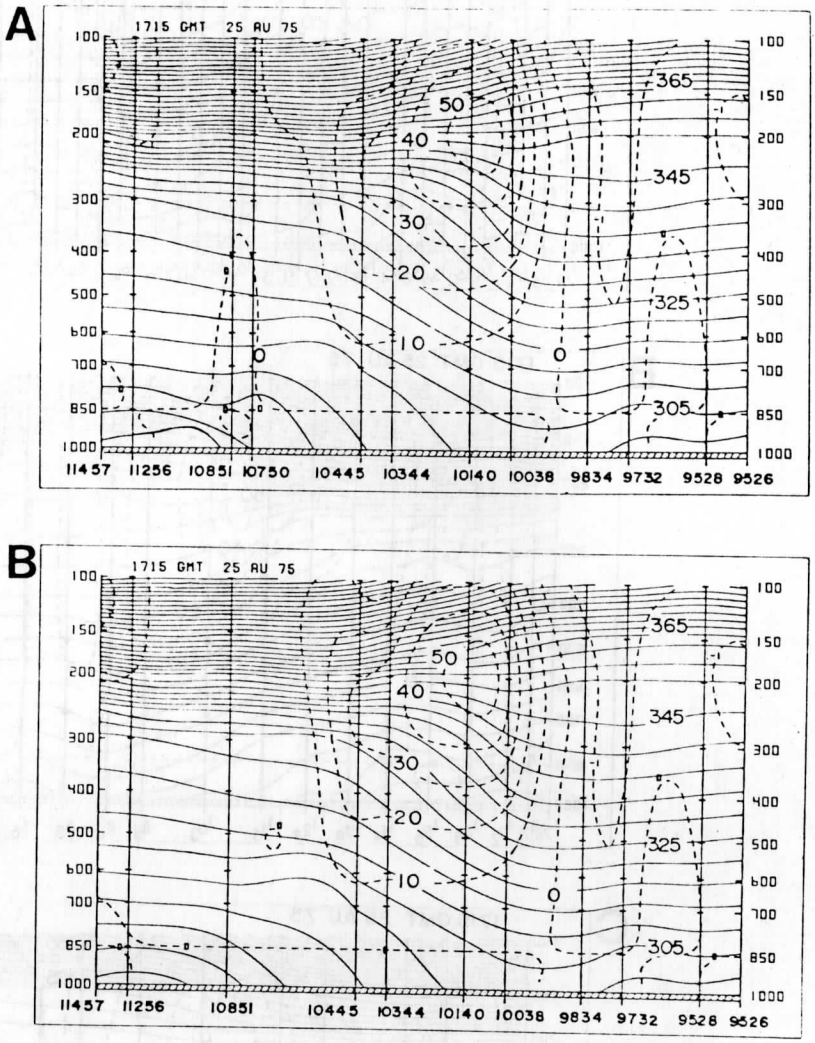

Figure 12. Western DST cross section.
(A) 1715 GMT 25 August 1975 unscreened.
(B) 1715 GMT 25 August 1975 after screening.

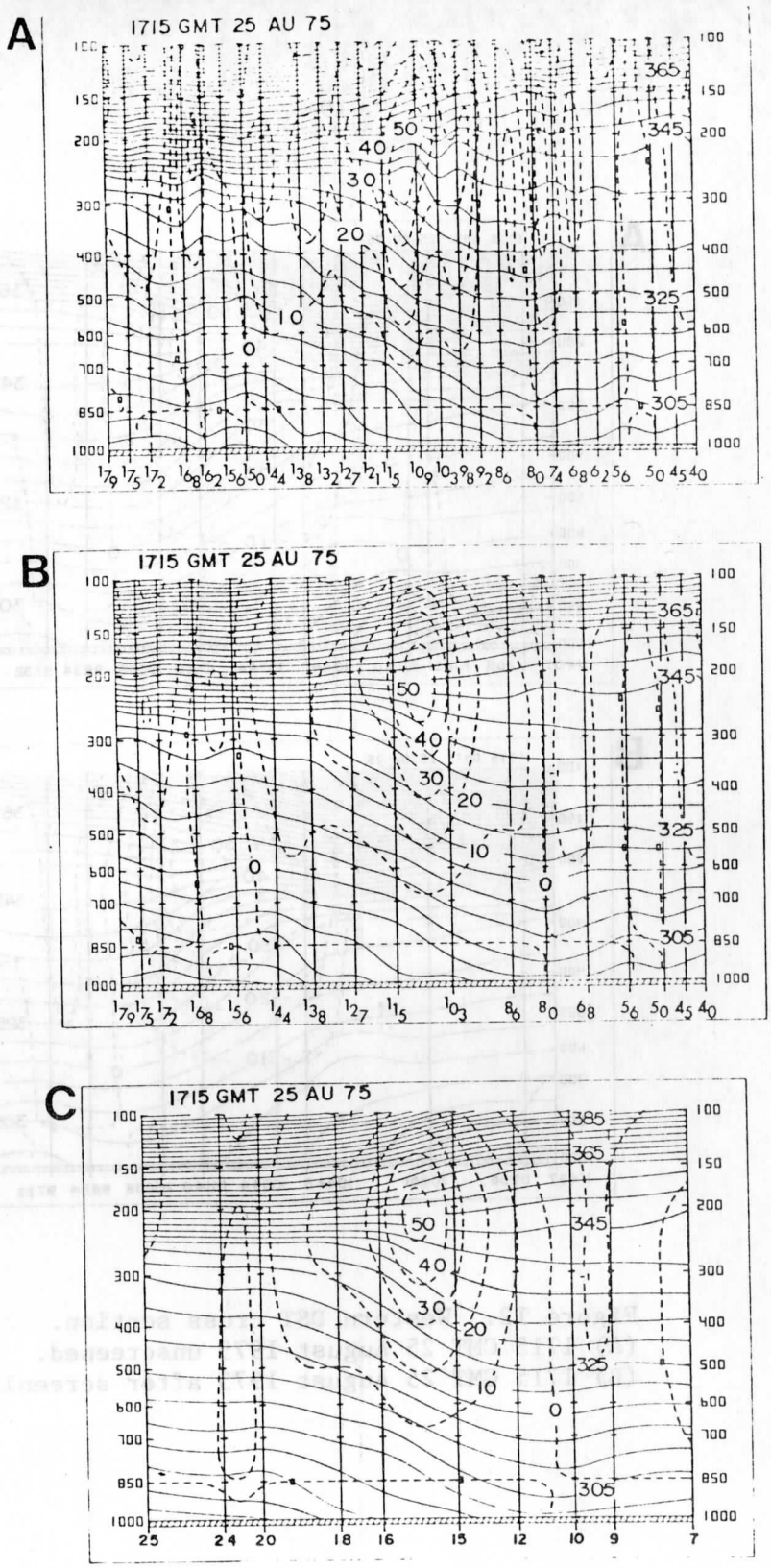

Figure 13. Western 4x7 cross section.
(A) 1715 GMT 25 August 1975 unscreened.
(B) 1715 GMT 25 August 1975 after screening.
(C) 1715 GMT 25 August 1975 DST-like average scheme.

to discover poor data, beginning with the most visible source of error, cloud cover. Less visible factors such as emissivities and instrument noise can also contribute. Consequently, it is advantageous to construct a series of cross sections through the area. (Petersen, 1977) Such a set of cross sections usually reveal inconsistent data because isentropes are very susceptible to poor data in the isentropic pattern. After viewing a series of cross sections and considering factors such as those mentioned above, the analyst decides which points are poor data. In the western 4 x 7 cross section, point 162 was in an area of high cloud cover and was removed. Points 150, 132, 121, 109, 98, 92 and 74 were also removed because of clouds or in some cases simply because they obviously were inconsistent although the reason was not apparent.

The jet core features shown in Figure 13b (i.e., after screening) are a close match to the 0000 GMT radiosonde cross section: 50 m s^{-1} core at 41.4°. The 1715 GMT satellite data produces an isotach pattern which has the compactness of the 1200 GMT radiosonde cross section. This suggests that the spreading of the wind maximum occurred closer to 0000 GMT.

The final western cross section is produced from the screened 4 x 7 data which are then averaged using the DST scheme (Fig. 13c). This gave better results than the original DST data. Each of the three jet core features falls within the trend shown by the bracketing radiosonde cross sections. The oval core of 50 m s^{-1} is located at 41.8° and 210 mb.

As shown in Table 1, the higher resolution screened 4 x 7 soundings gave better results than the DST data which have been used in the various impact studies noted in the introduction.

b) The eastern cross section

The second or eastern cross section runs from Fort Smith to Lake Charles. It provides another test for the satellite data. The objective analysis of the 1200 GMT radiosonde data (Fig. 14a) again illustrates the necessity for screening radiosonde data with this technique. Sounding 72853 (Shilo) when plotted on a thermodynamic diagram appears reasonable - there are no superadiabatic layers. But when compared with its neighbors in an isentropic cross section, it is clear that the sounding is unrealistically warm. A very warm valley appears in the isentropes upwards of 500 mb. Moreover, since this station only reported at 1200 GMT, it was omitted. The

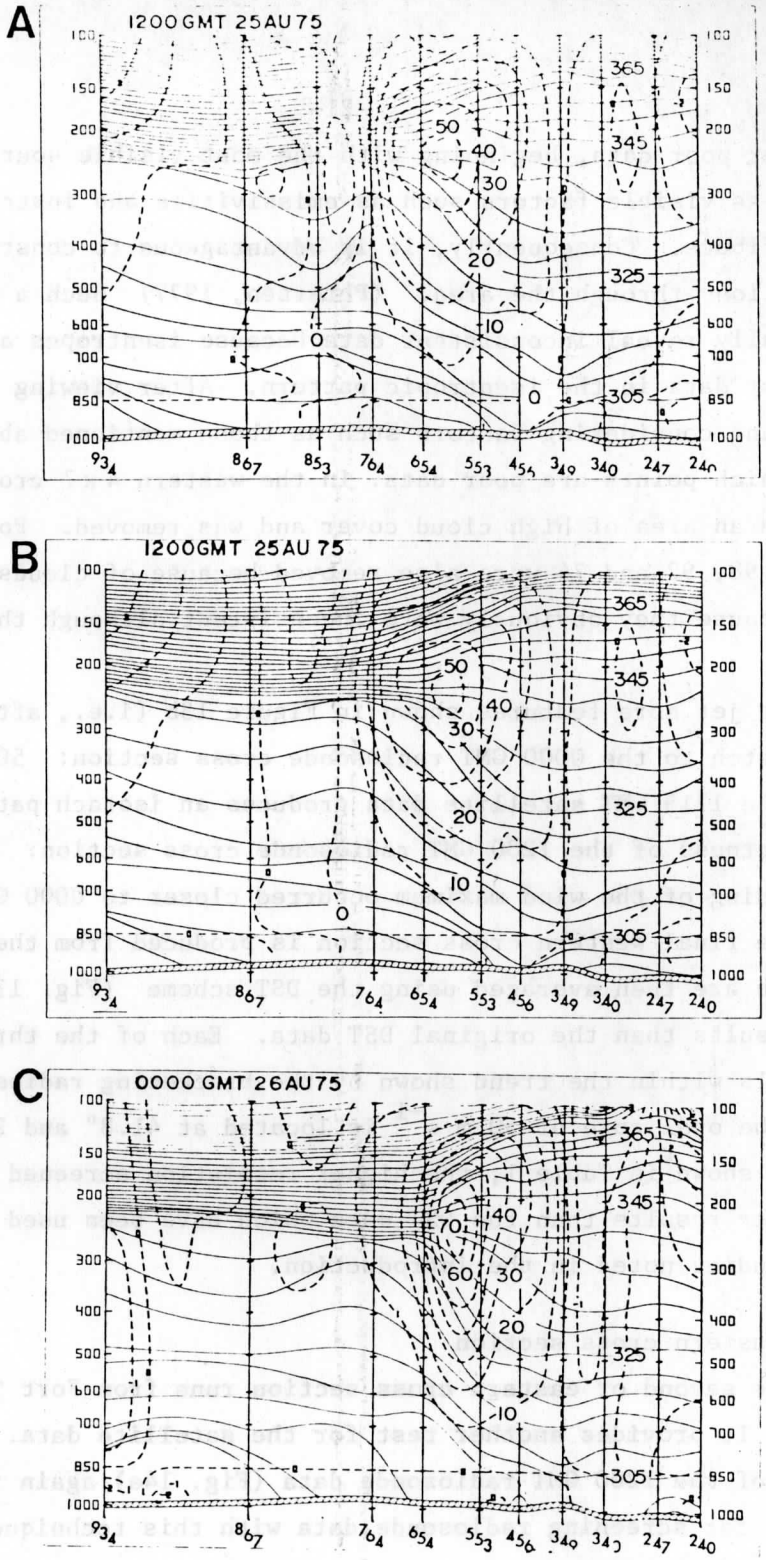

Figure 14. Eastern radiosonde cross section.
(A) 1200 GMT 25 August 1975 original.
(B) 1200 GMT 25 August 1975 corrected.
(C) 0000 GMT 26 August 1975.
Soundings are identified by station numbers - the 72 block prefix is omitted.

omission had no effect on the thermal support of the jet which was well to the south. The 1200 GMT cross section placed the 50 m s^{-1} core at 43.2° midway between Huron and Omaha at 250 mb. Twelve hours later, the baroclinity between Huron and Omaha sharply increased with the isentropes more steeply sloped and more tightly packed. The core pattern maximum of 70 m s^{-1} at 250 mb is sharply defined and located about 0.5° south of the 1200 GMT location. (See Fig. 14c.)

The objective cross section analysis of the DST data set reveals wind maxima at 43.4° and 39.5° (Fig. 15a); the problem occurs at the closely spaced soundings 10352 and 10351. As described earlier, to test which point was the bad one, west to east cross sections were made through 10352 and 10351. Point 10352 contained the apparently inconsistent data being much warmer than its neighbors and yielding a double jet core. An objective analysis omitting 10352 yielded a single 50 m s^{-1} core which was more compatible with the bracketing radiosondes. Overall, the DST cross section in Figure 15b shows a much smoother atmospheric structure than the radiosonde cross sections. Although the general shape of the wind core pattern and its maximum speed are fairly consistent with the bracketing radiosondes, the elevation is 50 mb higher. Even more important, the latitude of the thermal wind core is centered at 39.5°, almost 4° south of the radiosonde position. The DST data apparently failed to adequately capture the north-south temperature gradient.

Like the unscreened DST data, the raw 4 x 7 data produced two thermal wind maxima centered at latitude 43.5° and 39.6°. (Fig. 16a) The objective cross section analysis revealed an obviously warm pocket at point 93 above 800 mb. In addition, point 104 produces an apparently anomalous cold dome between 900 and 750 mb. Removal of points 93 and 104 produced the single 60 m s^{-1} core centered at 43.8° and 275 mb. (Fig. 16b) This position is now north of the 1200 GMT radiosonde position and 25 mb higher. The higher resolution 4 x 7 data captured the sharper baroclinity which moved the thermal wind core northwards.

Figure 16c (based on the DST-like data set) shows the central wind core at 42.2°, a northward movement of 2.7° over the original DST data. However, this is still 0.5° south of the 0000 GMT radiosonde location. (Refer to Table 2 which summarizes the results.) The 40 m s^{-1} core speed is weak compared to the estimated core speed from the radiosonde network, although

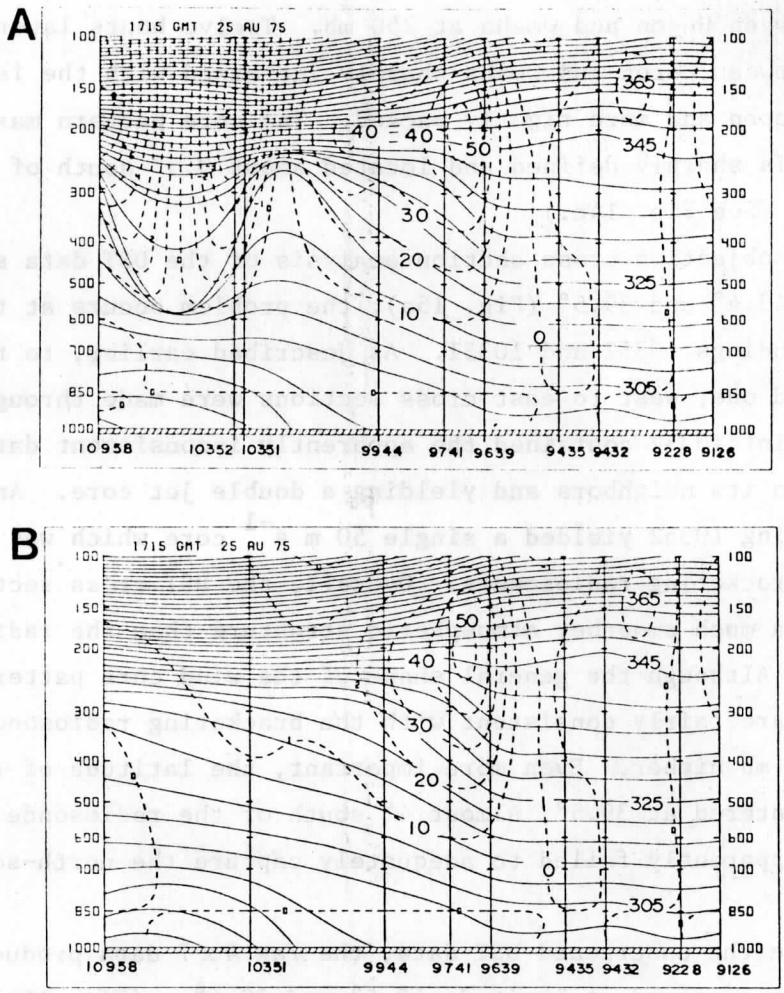

Figure 15. Eastern DST cross section.
(A) 1715 GMT 25 August 1975 unscreened.
(B) 1715 GMT 25 August 1975 after screening.

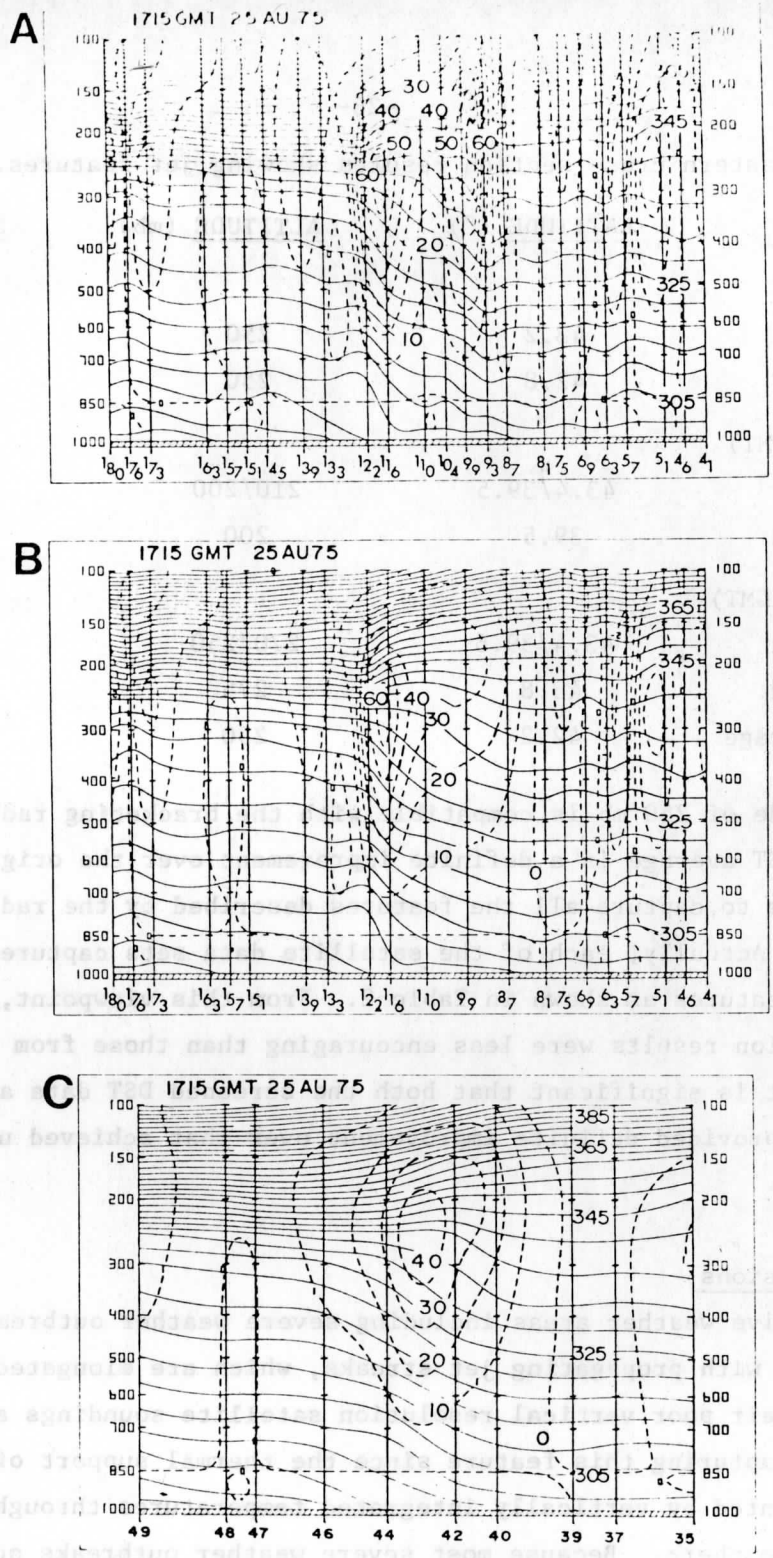

Figure 16. Eastern 4x7 cross section.
(A) 1715 GMT 25 August 1975 unscreened.
(B) 1715 GMT 25 August 1975 after screening.
(C) 1715 GMT 25 August 1975 DST-like average scheme.

Table 2. Eastern cross section results showing jet features.

TEST	LATITUDE (°)	ALTITUDE (mb)	SPEED (m s^{-1})
RADIOSONDE			
1200 GMT	43.2	250	50
0000 GMT	42.8	250	70
DST (1715 GMT)			
Original	43.4/39.5	210/200	40/50
Screened	39.5	200	50
4 x 7 (1715 GMT)			
Original	43.4/39.6	270/250	60/50
Screened	43.8	275	60
DST Average	42.2	250	40

the altitude of 250 mb is compatible with the bracketing radiosondes. While the 4 x 7 DST average is a definite improvement over the original DST set, it still fails to capture all the features described by the radiosonde cross sections. Actually, each of the satellite data sets captured only one of the main features as shown in Table 2. From this viewpoint, the eastern cross section results were less encouraging than those from the western case. However, it is significant that both the screened DST data and the screened 4 x 7 data provided definite improvement over that achieved using unscreened DST data.

7. Conclusions

Active weather areas including severe weather outbreaks are commonly associated with propagating jet streaks, which are elongated wind maxima. Despite their poor vertical resolution satellite soundings are particularly adept at capturing this feature since the thermal support of a jet streak is represented by vertically integrated temperatures through a large depth of the atmosphere. Because most severe weather outbreaks occur between the current radiosonde ascents at 1200 and 0000 GMT, a satellite capable of sounding at midday, or even better at any time of the day or night, provides an important time advantage to forecasters in keeping abreast of rapidly changing weather patterns. Since satellite soundings are often more closely spaced than the radiosonde stations, they can offer the higher resolution

needed to capture the long narrow jet core which can slip between radiosonde stations.

This study investigated the performance of satellite data sets in describing the thermal field beneath a jet streak. The comparison was made between Nimbus-6 data at approximately 1700 GMT and bracketing radiosonde cross sections on the severe weather day of 25-26 August 1975. The success of the satellite data was determined by how well it captured the latitude, altitude and intensity of the thermal wind core.

The satellite cross sections were based both on Data System Test (DST) soundings and the higher resolution 4 x 7 soundings. Two cross sections - an eastern and a western - were prepared for both data sets. In general, the DST cross sections provided somewhat disappointing results, even after the obviously poor DST soundings were removed. The thermal wind core was positioned 2.0 to 3.5° of latitude too far south.

Use of unscreened 4 x 7 soundings produced much noisier cross sections than the DST sections. However, after screening western cross section revealed a thermal wind maxima which agreed well with the bracketing radiosonde cross sections in latitude, altitude and maximum speed. On the other hand, the screened 4 x 7 eastern cross section produced a wind maximum slightly north (less than 1.0° of latitude) of the radiosonde cross section. However this location was considerably better than the DST which positioned the thermal wind core more than 3.0° too far south.

Since the DST data are based on averages from the 4 x 7 data set, they are affected by the quality of the higher resolution soundings. Consequently, it is reasonable to examine DST-like soundings which are obtained from the screened 4 x 7 data. This led to a definite improvement over the original DST data. The western cross section results produced a wind maximum that had characteristics consistent with the two bracketing radiosondes. While the eastern cross section based on the recombined 4 x 7 data did not capture the strengthening trend of the wind core seen in the radiosonde data, it did improve the altitude and latitude of the wind core compared to those in the original DST data.

While radiosonde data are not necessarily capable of locating the true position of a jet maximum and its thermal support, they have been used as a standard for verification in this thesis. However, the fact that the screened satellite data positioned the thermal wind maximum much closer to

the radiosonde location than the unscreened data indicates that the radiosonde data provide a very reasonable estimate of the true position.

The main thrust of this study was to find if a higher resolution data set would be superior to the commonly used DST soundings in locating jet maxima. This appears to have been accomplished. However the use of an objective analysis technique to screen poor soundings that had passed the routine quality checks was important in this success. Such screening produces marked improvement, especially in defining wind core characteristics with 4 x 7 data. As a secondary benefit, the recombination of 4 x 7 data with the DST averaging scheme after careful screening also shows marked improvement in defining wind cores with this lower resolution data set.

The fact that the screened 4 x 7 Nimbus-6 data were able to improve on the DST data in locating the thermal support of the jet streak indicates that good-quality and higher-resolution satellite data can be a useful tool to the field forecaster, and this information would be especially useful in off-radiosonde hours. Finally, it should be noted that 4 x 7 soundings are themselves averages of up to 28 individual soundings. Consequently, further improvement might be attained by quality checking a limited number of the 28 soundings that make up each 4 x 7 array.

References

Achtor, T.H. and L.H. Horn, 1981: The role of the upper tropospheric jet streak, 850 mb winds and static stability in springtime Colorado cyclogenesis. NOAA Project Report (in press).

Danielsen, E.F., 1959: The laminar structure of the atmosphere and its relation to the concept of tropopause. Arch. Meteor. Geophys. Bioklim., A11, 293-332.

Duquet, R., Danielsen, E.F., and N.R. Phares, 1966: Objective cross section analysis. J. Appl. Meteor., 5, 233-245.

Horn, L.H., Petersen, R.A., and T.M. Whittaker, 1976: Intercomparisons of data derived from Nimbus-6 temperature profiles, rawinsonde observations and initialized LFM model fields, Mon. Wea. Rev., 104, 1361-71.

Hovanec, R.D. and L.H. Horn, 1975: Static stability and the 300 mb isotach field in the Colorado cyclogenetic area. Mon. Wea. Rev., 103, 628-638.

Kapela, A. and L.H. Horn, 1975: Nimbus-5 satellite soundings in a strongly baroclinic region, Meteorological Applications of Satellite Indirect Soundings, Project Report, NOAA Grant 04-4-158-2, Dept. of Meteorology, University of Wisconsin, Madison. Also presented in part as an invited paper at the 16th General Assembly of IUGG, Grenoble, France.

Marshment, R.A. and L.H. Horn, 1981: Moisture distribution and its evolution during spring season Colorado cyclogenesis, NOAA Project Report (in press).

NASA, 1975: Nimbus-6 User's Guide; Goddard Space Flight Center, Greenbelt, MD.

Newton, C.W., 1954: Frontogenesis and frontolysis as a three dimensional process. J. Meteor., 11, 449-461.

Palmen, E. and C.W. Newton, 1969: Atmospheric Circulation Systems, Academic Press, New York, 603 pp.

Petersen, R.A., 1977: Three-dimensional objective analysis based on isentropic cross-sectional techniques. Meteorological Applications of Satellite Indirect Soundings II, Univ. of Wisc. Project Report, 8-54.

_____, and L.H. Horn, 1977: An evaluation of 500 mb height and geostrophic wind fields derived from Nimbus-6 soundings. Bull. Amer. Meteor. Soc., 58, 1195-1201.

Sechrist, F. and D.R. Johnson, 1970: On the isentropic representation of storms, dynamic destabilization and squall line formation. 51st Annual Meeting Amer. Geophys. Union, Wash., D.C., Abstract, EOS Transaction, A.G.U., 51, 4, 294.

Shapiro, M.A. and J.T. Hastings, 1973: Objective cross-section analyses by Hermite polynomial interpolation on isentropic surfaces. J. Appl. Meteor., 12, 753-762.

Smith, W.L. and H.M. Woolf, 1976: The use of eigenvectors of statistical covariance matrices for interpreting satellite sounding radiometer observations. J. Atmos. Sci., 33, 1127-1140.

Togstad, W.E. and L.H. Horn, 1974: An application of the satellite indirect sounding technique in describing the hyperbaroclinic zone of a jet streak. J. Appl. Meteor., 13, 264-276.

Trewartha, G. and L.H. Horn, 1980: Introduction to Climate, 5th Edition, McGraw-Hill Book Co., New York City, N.Y., 416 pp.

Uccellini, L.W. and D.R. Johnson, 1979: The coupling of upper and lower tropospheric jet streaks and the implications for the development of severe convective storms. Mon. Wea. Rev., 107, 682-703.

Whittaker, T.M. and R.A. Petersen, 1977: Objective cross-sectional analyses incorporating thermal enhancement of the observed winds, Mon. Wea. Rev., 105, 147-153.

Winston, J. (editor), 1956: Forecasting tornadoes and severe thunderstorms, Forecasting Guide No. 1. U.S. Weather Bureau, Dept. of Commerce, Wash., D.C., 34 pp.

Nimbus-6 Temperature Soundings Obtained Using Interactive Video-Graphics Computer Techniques

Byron A. Paulson* and Lyle H. Horn
Department of Meteorology, University of Wisconsin-Madison
Madison, Wis. 53706

Abstract

In an attempt to improve the quality of Nimbus-6 soundings the Man-computer Interactive Data Access System (McIDAS) at the University of Wisconsin is used to manually edit individual (scan spot) High-resolution Infrared Sounder (HIRS) soundings. Unlike the Nimbus-6 Data System Test (DST) soundings which are derived from averages of up to 84 spot radiance measurements and the TIROS-N and NOAA-6 operational soundings which can involve averages of up to 63 spot measurements, the HIRS soundings used in this study are derived from single spot radiances or averages of five single spot soundings. Also, unlike the DST soundings, the HIRS McIDAS retrievals used contemporary surface (instrument shelter) temperatures as a pseudo-infrared window channel to aid in cloud filtering. These McIDAS generated soundings are used to analyze: 1) level temperature fields at 850, 500, and 300 mb, 2) the 850-300 mb thickness field and 3) the 500 mb height field over eastern Europe for an August 20, 1975 case. The excellent radiosonde network in this area is used for verification purposes.

While the individual spot soundings offer little improvement over the DST data, the averages of five of these soundings provide analyses which are distinctly superior to the operational DST soundings. Although improvement is noted in the root mean square and bias scores, the largest improvements are found in the S1 score which is a measure of gradient comparison. The radiosonde verification data are partitioned into subsets and in some tests are combined with the HIRS soundings. Other tests involve comparisons in which the radiosonde data consist of only mandatory level data. The various tests indicate that the edited HIRS soundings averaged in small groups are comparable to mandatory level radiosonde data in constructing 500 mb height analyses.

*Present affiliation, National Weather Service, Minneapolis, Minnesota

1. Introduction

Vertical temperature profiles retrieved from satellite measured radiances have been an important component of the GARP (Global Atmospheric Research Program) observational system. Although satellite soundings have the potential for providing the global data needed for operational numerical prediction models, their effectiveness has been inconclusive. Impact studies conducted by the National Meteorological Center (NMC) have indicated that the inclusion of satellite soundings into the NMC data base did not improve the numerical model forecasts (Tracton et al., 1980). On the other hand, Ghil et al. (1979) and Kelly et al. (1978) have reported some forecast improvement when Nimbus-6 satellite sounding data were included as input for the National Aeronautics and Space Administration and Australian Numerical Research Centre prediction models, respectively. While the ultimate test of the effectiveness of satellite soundings will be their ability to improve numerical weather predictions, it is difficult to evaluate these new data when they are combined with radiosonde and other meteorological data in complex numerical models.

Because of the difficulty of assessing the quality of satellite soundings, it is important that they be evaluated in studies which directly reveal their strengths and limitations. For example, Phillips et al. (1979) recently used TIROS-N satellite soundings with co-located radiosonde observations to study some of the peculiarities of the satellite soundings, particularly their error characteristics under varying degrees of cloudiness. Another approach is to compare descriptions of synoptic features obtained from only satellite sounding data with those obtained from only radiosonde data. The primary focus in these studies is on comparisons of gradients obtained from the two data sets. Horn et al. (1976) found that Nimbus-5 soundings used alone were capable of describing the intense thermal gradient beneath an upper tropospheric jet streak, while Petersen and Horn (1977) successfully used Nimbus-6 soundings to track a 500 mb low. In both studies success was in part attributed to <u>screening</u> of the satellite soundings, eliminating obviously poor data. Despite "clear column" techniques developed by the National Environmental Satellite Service (NESS) to reduce the effects of clouds, most poor soundings result from cloud contamination of the infrared radiances.

The satellite soundings screened in the studies noted above were part of the Data System Test (DST) data base produced by NESS as a forerunner to the current TIROS-N and NOAA-6 operation. Each DST sounding uses an objectively derived average of many individual radiance measurements, theoretically as many

as 84. Because improved results were obtained by screening these averaged data, it was decided to determine if even greater improvement might be achieved by manually screening individual data before averaging, rather than using a purely objective scheme.

This report focuses on the improvements achieved in the Nimbus-6 soundings when manually edited spot soundings are used either individually or in small groups (up to five spots) to obtain an "operational" sounding. This objective is in accordance with the GARP "Special Effort" recommendation that attempts be made to achieve the highest possible horizontal resolution in the sounding data (Greaves et al., 1979). It should be added that the NESS Mesoscale Applications Group at the University of Wisconsin-Madison is employing a somewhat similar procedure, constructing TIROS-N and NOAA-6 operational soundings from the averages of up to nine spots.

The edited Nimbus-6 soundings obtained in this study are tested by using them to construct 850, 500 and 300 mb level temperature fields, an 850-300 mb thickness field and 500 mb height fields, which are compared with fields obtained from radiosonde data. Nimbus-6 data gathered over central and eastern Europe on August 20, 1975 are used. This area was chosen because its dense radiosonde network provides an excellent verification data set. The satellite passage occurred near radiosonde time and during a period when all channels of the Nimbus-6 infrared sounder were operational. Since the infrared sounder aboard Nimbus-6 and the processing procedures are essentially the same as those of TIROS-N and NOAA-6, the results achieved here very likely also apply to the current polar orbiting sounders. Before describing the editing method and its results, it is important to briefly review the Nimbus-6 instrument and retrieval procedures.

2. Instruments and retrieval procedures

Nimbus-6, launched 12 June 1975 into a nearly sun-synchronous orbit of 1100 kilometers, carried two sounding instruments: the High-resolution Infrared Sounder (HIRS) and the Scanning Microwave Spectrometer (SCAMS). HIRS provides radiance measurements in 17 spectral bands, seven in the 15 micrometer region, five in the 4.3 micrometer region, with the remainder in window regions and water vapor bands. The HIRS instrument scans perpendicular to its orbital path, 36.9° to the right and left, which on the earth's surface amounts to about 825 km on either side of the nadir path. At the subsatellite point the ground resolution of individual HIRS field of view is approximately 30 km.

The SCAMS instrument has five channels which measure microwave radiances, three in the spectral band near 0.5 cm for temperature sounding, and two near

0.2 cm for moisture sounding. The instrument scans 43.2° to the right and left of its orbital path in 7.2° steps. Since it measures less intense radiation than HIRS, it requires a larger field of view, approximately 145 km at nadir. However, the SCAMS has an advantage in that it is not significantly affected by non-precipitating clouds. See the Nimbus-6 Users Guide (1975) for more complete descriptions of the instruments.

In order to appreciate the editing procedure used in this study, it is first necessary to understand the manner in which the Nimbus-6 soundings were processed for the DST. In one scan (left and right of its orbit), HIRS measures radiances in 42 fields of view. (See Fig. 1.) After completing 20 such scans, HIRS enters a calibration mode causing a short gap in transmission. These 840 fields of view (42 x 20), could, under ideal conditions, produce 840 individual soundings roughly 30 km apart. However, factors such as clouds, varying surface emissivities, pronounced surface elevation changes, and instrument noise cause some of the radiances to be unsuitable for temperature retrievals.

Because such a dense array of individual soundings is unmanageable and impractical for most purposes, NESS divided each 840 member array into thirty subsets of 4 x 7 fields of view, (four along the orbital path by seven across the path). Within a 4 x 7 block, each individual HIRS measurement is checked for consistency (and possibly discarded) using SCAMS measurements interpolated to the HIRS fields of view. (Recall that SCAMS radiances are not degraded by non-precipitating clouds.) Acceptable radiances are then combined in a manner described by Smith and Woolf (1976). Their method, designed to minimize the effect of cloud contamination, yields a set of clear column (cloud-free) infrared radiances representative of the 4 x 7 block. In the example shown in Fig. 1, the 4 x 7 blocks marked with X's have cloud-free infrared radiances suitable for retrieving vertical temperature profiles. These cloud free infrared radiances are supplemented with SCAMS radiances interpolated to the cloud-free radiance locations. In the basic DST data set, NESS furnished a sounding at each of these locations.

During the DST processing of the satellite retrievals, the National Meteorological Center (NMC) found that the number of 4 x 7 soundings (up to 30 between calibration intervals) was too large to handle in operational work. A maximum of 12 soundings was chosen as manageable, which resulted in a further averaging of the 4 x 7 arrays. The center location of the final averages is shown by the squares in Figure 1. These averaged radiances and the eigenvector

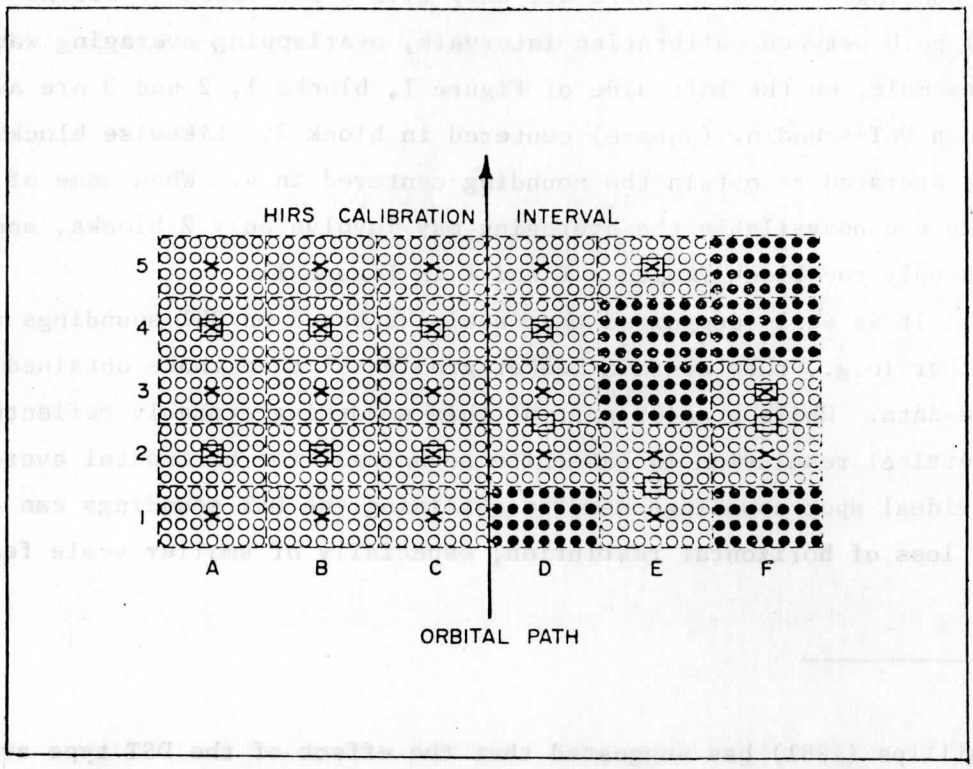

Figure 1. A schematic of HIRS data averaging. Circles represent individual HIRS fields of view. In this example, shaded circles indicate fields of view not used because of cloud contamination. Dashed lines outline HIRS 4x7 blocks. The 4x7 soundings are located by X's. The DST soundings, based on overlapping averaging of 4x7 blocks, are indicated by squares (□). At A-4, the DST sounding consists of the averages of the A-5, 4 and 3 blocks, while the DST sounding at E-5 consists of only one 4x7 block because of cloud contamination in adjacent regions.

approach described by Smith and Woolf (1976) were used to retrieve the so-called DST soundings. Because there are only five 4 x 7 radiance blocks along the orbital path between calibration intervals, overlapping averaging was required. For example, on the left side of Figure 1, blocks 1, 2 and 3 are averaged to yield a DST sounding (square) centered in block 2. Likewise blocks 3, 4 and 5 are averaged to obtain the sounding centered in 4. When some of the 4 x 7 blocks are unavailable the averaging may involve only 2 blocks, and in some cases only one block (Columns E and F in Figure 1).

It is well-recognized that analyses based on DST soundings are usually smoother (e.g., they contain weaker gradients) than those obtained from radiosonde data. While a major part of this smoothing probably reflects the lack of vertical resolution in satellite soundings, the horizontal averaging of many individual spot soundings used in obtaining the DST soundings can contribute to some loss of horizontal resolution, especially of smaller scale features.[1]

---

[1] Phillips (1981) has suggested that the effect of the DST type averaging on the loss of variance should be estimated using analytical equations. Assume an original temperature distribution (T),

$$T = A \cos\left(\frac{2\pi x}{L}\right)$$

where A is amplitude, x is the distance coordinate and L is wave length. A smoothed function of T, denoted as T_s, obtained from employing soundings averaged over an incremental distance Δ is given by,

$$T_s = \frac{1}{\Delta}\int_{x-\frac{\Delta}{2}}^{x+\frac{\Delta}{2}} T\,dx = \frac{\sin\varepsilon}{\varepsilon}\,T \quad , \text{ where } \quad \varepsilon = \frac{\pi\Delta}{L} \quad .$$

Considering the DST averaging (including overlapping), calibration gaps etc, the DST soundings are about 300 km apart in regions of clear skies. Using Δ = 300 km and L = 3000 km, $T_s = 0.984\,T$, which represents a very small loss of variance. However for Δ = 300 km and L = 1000 km, $T_s = 0.858\,T$ which indicates an appreciable loss of variance in this ideal analytical field.

3. Alternate selection procedures

A major goal of this study is to determine whether the quality of satellite soundings can be improved through manual selection and limited averaging of individual soundings (fields of view). Individual soundings were selected using the University of Wisconsin's video graphics Man-computer Interactive Data Access System (McIDAS). The manually selected soundings obtained in this study were based on the same radiance measurements used in the DST soundings; however, the temperature profile retrievals made using McIDAS were based on a simple regression approach rather than the eigenvector method employed in obtaining DST soundings (Smith et al., 1979). The regression coefficients were calculated from the radiosonde and radiance data collected over Europe during the entire DST-6 period of 18 August to 4 September 1975, which includes the August 20 case examined here. The McIDAS retrieval algorithm, unlike the DST retrieval algorithm, employed contemporary surface (instrument shelter) temperatures. (It should be noted that the DST also used surface temperatures but they were 24 hours old.) In this study the contemporary surface temperatures were treated as a pseudo-infrared window channel during the McIDAS retrieval procedure and thus aided in filtering cloud contamination. The effect of this pseudo-channel should provide improved soundings in the lowest layers (i.e., below 850 mb). However, as will be noted later in the paper the existence of strong nocturnal temperature inversions over much of the study area may have partially offset the positive influence of this pseudo-surface channel.

The McIDAS retrievals were made from two consecutive orbits over eastern and central Europe. The westernmost orbit brought the satellite over the region at about 2330 GMT 20 August 1975; the adjacent orbit to the east occurred about 107 minutes earlier. Figure 2 (straight dashed lines) shows the area encompassed by the two orbits. Because of the relatively high latitude, data were lacking for only a small wedged-shaped area between orbits (just north of the Black Sea). Soundings from both orbits were analyzed together, neglecting the time difference. In comparing satellite soundings with the 0000 GMT radiosonde data, the time differences of an hour or two was neglected. This is a fair approximation since about 45 minutes are required for a typical radiosonde ascent to 100 mb.

As a first step in obtaining HIRS temperature retrievals a radiance field having the appearance of a mosaic is displayed on the McIDAS video screen. Normally the radiance field of a channel with its peak energy contribution near the surface is first displayed. Those 30 km HIRS fields of view (pixels) of the mosaic that are darker (warmer brightness temperature) than their surroundings

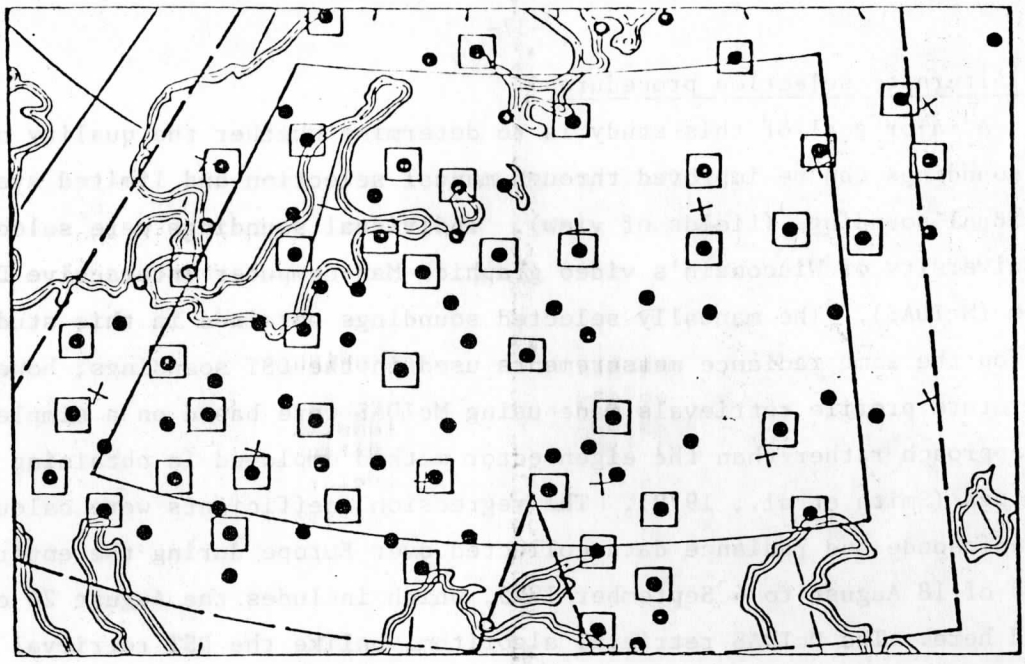

Figure 2. Area of study. Dashed lines indicate area in which retrievals were made from two orbits of Nimbus-6. Solid interior lines denote analysis area. Circles indicate radiosonde station locations. Stations with boxes around circles are locations of the Reduced Radiosonde Network (RR1). Remaining circles represented the RR2 network. See text.

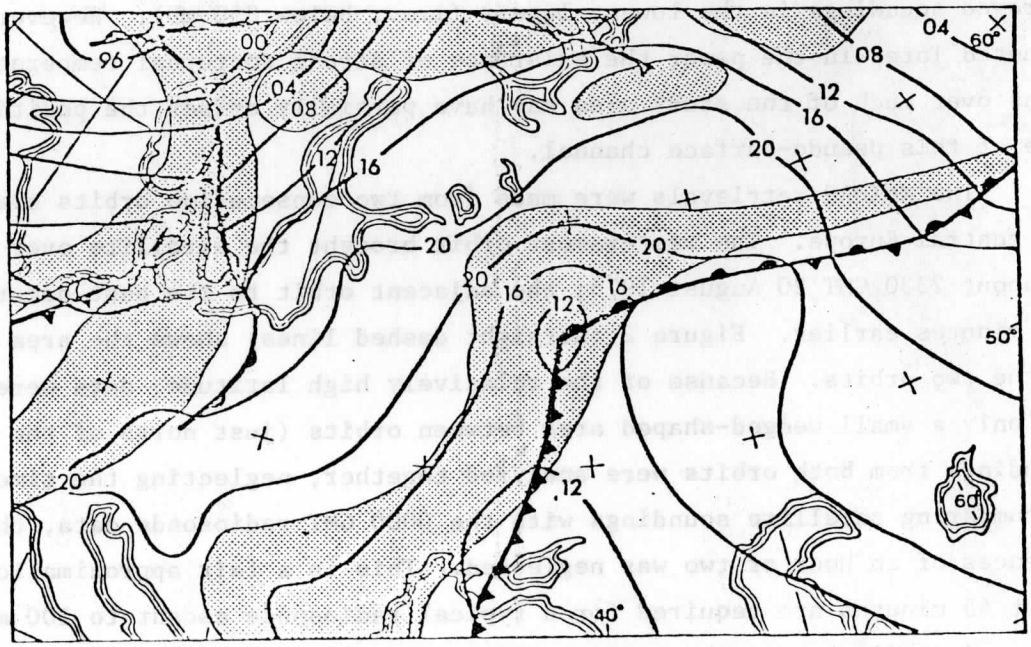

Figure 3. Surface analysis for 0000 GMT August 21, 1975. Stipling indicates principal areas of cloudiness.

are generally cloud free and good candidates for temperature retrievals. Because of the relatively small size of these fields of view, the operator can obtain soundings through breaks in a mostly overcast region. If this is not possible, the retrieval algorithm will employ a partly cloudy N-star technique (Smith, 1968) to derive a clear column radiance from two adjacent fields of view.

The McIDAS operator selects a pixel for which a temperature profile is desired. An algorithm interpolates a SCAMS measurement to the HIRS field of view, and the following data are displayed on the screen: 1) the HIRS retrieved temperature at each mandatory level (1000, 850, 700, 500, 400, 300, 250, 200, 150 and 100 mb); 2) the temperature difference between the HIRS and SCAMS derived temperature at each mandatory level to 300 mb; and 3) the vertically summed RMS (root mean square) temperature difference between HIRS and SCAMS over the mandatory levels to 300 mb. The HIRS-SCAMS differences are used as the first step in the editing process.

McIDAS is also programmed to analyze the fields of retrieved temperature at the mandatory levels or the fields of brightness temperature for various radiance channels. Thus the operator can quickly select, examine, analyze, and edit retrievals.

To construct fields of retrieved temperature, soundings are generally first attempted in obviously clear areas (i.e., warm brightness temperatures). Then the operator attempts retrievals in areas of partial cloud cover. After acquiring a sufficient number of temperature retrievals, McIDAS can be used to display the isotherm analysis to aid in eliminating inconsistent retrievals. The 500 mb level was usually used in this editing since it is above much of the low cloudiness and yet below the tropopause. However, a small amount of editing was also done at 850 and 300 mb. Once the operator is satisfied with the consistency of the analysis displayed on McIDAS, the soundings on which the analysis is based are retained as the data set. At no time during the selection and editing process were radiosonde data or surface temperatures used.

4. Data sets

Several sets of HIRS soundings were retrieved using the selection methods described in the previous section, but only two are examined in this paper. These soundings were "dry"; i.e., moisture data were not included. In addition to the two HIRS data sets, results obtained from the DST and a set of microwave (SCAMS) soundings are included. Use of the DST set provides some insight into

the data quality used in the numerical model impact studies mentioned in the introduction. The SCAMS soundings are included since they were used as an aid in editing the individual HIRS soundings, and because they are based on radiances not affected by non-precipitating clouds. Verification was accomplished using a network of 96 radiosonde stations in the area of study. As will be discussed later, the radiosonde data set was modified to provide additional insight into the characteristics and quality of the satellite data. The various data sets, both satellite and radiosonde verification data, are described below.

a) Data System Test (DST) soundings

The manner in which the 76 DST soundings within the area of study were retrieved by NESS was described in detail in section 2. As noted previously, the DST sounding retrievals were obtained using the eigenvector procedure, while the HIRS soundings of this study are based on regression retrievals. Thus comparisons between the HIRS data sets and the original DST soundings are not entirely unequivocal.

b) Manual (MAN) retrievals

The manual editing procedure yielded a total of 335 HIRS soundings, each based on a single field of view. The McIDAS operator (Paulson) attempted these retrievals in cloud-free regions. Because of the small field of view (30 km) some of these soundings (henceforth called the MAN set) were also accomplished in breaks in generally cloudy regions. The 335 MAN soundings were distributed rather uniformly across the study area.

c) Group Co-located (GCL) soundings

Next, a set of HIRS soundings located near radiosonde stations was produced. It was anticipated that these nearly co-located soundings would facilitate satellite-radiosonde comparisons. Initially, between 5 and 15 retrievals were made within about 70 km of each radiosonde station. These soundings were edited on McIDAS until only one representative sounding remained. (It should again be emphasized that radiosonde data were not used in the editing.) These single soundings (93 in number) were essentially co-located with radiosonde stations. Analyses based on these retrievals showed some improvement over those based on the 335 MAN retrievals. The lack of truly significant improvement appeared to be due to noise present in data sets based on single fields of view, even after editing. Consequently, about five soundings within a 70 km radius of each radiosonde station were retained. A Cressman-type weighting procedure was used to interpolate these retrievals to the radiosonde station location,

thus providing a single weighted sounding. (The University of Wisconsin's UNIVAC 1110 rather than McIDAS was used in the interpolation.) In the case of three of the 96 radiosonde station locations extensive cloudiness was present so no HIRS retrievals were achieved. The 93 soundings will be called the Group Co-located (GCL) set.

d) Microwave retrievals (MWD)

Since part of the editing procedure used in the HIRS retrievals involves comparisons with the SCAMS retrievals, it was decided to examine the results that could have been achieved using only microwave data. This data set will be referred to as the MWD set. The microwave temperatures examined here were SCAMS retrievals interpolated to HIRS MAN sounding locations. Thus, temperatures from more than one SCAMS retrieval were often incorporated into a MWR sounding. A total of 335 such microwave soundings were generated, one for each MAN location.

e) Radiosonde data sets (CRB, RR1, RR2)

A total of 96 radiosonde stations were located within the region of study (Fig. 2). The 0000 GMT 21 August 1975 observations at those stations were used as a verification standard with which to compare the satellite data sets. While it is well recognized that radiosonde observations are not error-free, they nevertheless provide the best verification available. This set of radiosonde observations which include both mandatory and significant level data will be referred to as the Complete Radiosonde (CRB) set.

To examine the effect of the density of the data network on the results and to conduct experiments in which the satellite and radiosonde data are mixed, a subset consisting of one-half (48) of the radiosonde stations was selected. To make this subset more comparable to satellite data, only dry, mandatory level radiosonde data were used. This set, referred to as the Reduced Radiosonde One (RR1) set, was obtained by asking a student unfamiliar with the research to select one-half of the radiosonde stations in such a way as to insure relatively uniform spacing. (See Fig. 2.) The remaining 48 radiosonde stations, not as uniformly spaced, will be called the Reduced Radiosonde Two (RR2) set. The RR2 set also consisted of only dry mandatory level data.

f) Combined Radiosonde-Satellite data sets (RS1, RS2)

In a final experiment, radiosonde data from the 48 radiosonde stations of the RR1 set were combined with GCL satellite data at the missing 48 radiosonde stations (i.e., the RR2 locations) to form a combined radiosonde-satellite data set. This combined set will be called the RS1 set. A similar set obtained by combining radiosonde data from the RR2 set with GCL satellite data at missing

radiosonde locations (i.e., at the 48 RR1 locations), will be referred to as the RS2 set.

5. Analysis procedures and experiment design

The effectiveness of the McIDAS editing procedure was tested by comparing analyses based on the various satellite data sets with those obtained using only radiosonde data. Comparisons were done for: 1) the temperature fields at 850, 500, and 300 mb, 2) the 850-300 mb thickness field and 3) the 500 mb height field. Each satellite data set and the reduced radiosonde networks were verified against the complete radiosonde network (CRB).

Analyses were done on a 1° latitude-longitude grid. Both satellite and radiosonde observations were interpolated to this grid using Cressman-type weights on the five observations nearest each grid point. (Whittaker, 1976.) To lessen boundary problems arising from these interpolations, the analysis grid was made a subset of the larger area in which satellite soundings were retrieved. See Fig. 2.

Verification was done using the grid point results to calculate the bias, root mean square difference (rms), and the S1 skill score. The S1 score, a measure of the difference between gradients, is commonly used to verify forecast gradients against observed gradients. The S1 score can range from 0 (perfect agreement) to 100. A score of 40 in a 24 hr 500 mb forecast is considered fair and a score of 20 is very good. In this study, gradients were calculated using a 2° latitude-longitude spacing (i.e., every other grid point). Because of the great importance of gradients in most meteorological problems, the S1 scores are given special significance.

6. Results

The discussion of the results achieved through the editing procedures will be organized around the three parameters noted earlier: temperature fields at 850, 500 and 300 mb, the thickness field of the 850-300 mb layer, and several derived 500 mb height fields. Representative maps of the 850 mb temperature and 500 mb height fields, and a complete set of tables showing the bias, root-mean-square differences and S1 scores for all comparisons will be presented.

Before examining the verification scores, a brief review of the general synoptic situation over central and eastern Europe at 0000 GMT 21 August 1975 is in order. The surface synoptic pattern (Fig. 3) shows a frontal cyclone centered over the USSR near 55°N, 40°E. A second cyclone is centered west of

Norway with its frontal system extending southeastward into Europe. The major areas of cloudiness shown by stipling in Fig. 3 are associated with the frontal zones. Visible and infrared images made from the NOAA-4 satellite aided in outlining these clouds. Of course, the McIDAS display of the infrared radiances of the HIRS channels, particularly those which peak at lower elevations, also reveal the presence of clouds. The 500 mb pattern for 0000 GMT can be seen in Fig. 6a. Its major feature consisted of a trough extending southward from Lake Ladoga into the Balkans. A ridge extended north-northeastward from the Alps to the Baltic Sea, with a second trough (not shown) west of Norway. All these late summer features were rather weak with the strongest 500 mb winds reaching only 25 m s^{-1}.

a) Level temperature verifications

Of all the parameters examined in this study, the level temperature retrievals probably provide the severest test for satellite data. Because of the relatively poor vertical resolution of satellite soundings, layer mean temperatures or thicknesses usually produce results closer to radiosonde data than do temperatures at a specified level. Table 1 summarizes the various data sets

TABLE 1

Level Temperature (°C) Comparisons

	850 mb			500 mb			300 mb		
DATA	RMS	BIAS	S1	RMS	BIAS	S1	RMS	BIAS	S1
CRB	VERIFICATION DATA SET								
DST	1.68°C	0.46°C	47.99	1.31°C	0.41°C	45.84	1.86°C	-1.12°C	50.73
MWD	1.92	-1.05	47.14	1.25	-0.12	43.75	1.60	-0.40	50.08
MAN	1.83	-1.09	44.92	1.41	0.29	44.70	1.08	0.21	44.05
GCL	1.49	-0.77	39.21	1.11	0.33	35.94	0.97	0.30	40.84
RR1	0.93	.09	34.89	0.65	0.21	32.00	0.73	0.07	38.57
RS1	0.88	- .36	27.55	0.57	0.22	23.07	0.61	0.11	29.66
RR2	1.95	0.40	46.12	1.03	-0.17	40.24	1.05	0.01	44.27
RS2	0.91	-0.45	26.50	0.84	0.14	29.42	0.70	0.20	27.42

and verification parameters for the level temperatures at 850, 500 and 300 mb. In general, the DST and microwave (MWD) soundings produced similar results when compared with the complete radiosonde data set (CRB). The manual (MAN) set has S1 scores that are a few points better than either the DST or MWD set, although the rms differences for the MAN set show no improvement. However, the Group

Co-located (GCL) HIRS soundings show marked improvement over the DST and MWD sets in both the rms and S1 comparisons, with the S1 scores showing about a 10 point improvement.

Figure 4 displays the objective analyses of the 850 mb temperature field achieved from the CRB, DST, MAN and GCL data sets. These analyses are qualitatively consistent with the scores achieved by the various satellite data sets. For example, the DST analysis lacks the gradients of the CRB set as the S1 score suggests. This has been a common feature in DST-radiosonde comparisons. On the other hand, the MAN set captures more of the gradients but provides a somewhat noisy isotherm pattern (high rms). This very likely results from the large number (335) of soundings used and the lack of averaging in this set. The GCL set which consists of averages of five single spot soundings provides a considerably improved field. The major gradients are described and the field is not noisy.

The improvement obtained using the GCL set over the MAN set can in part be attributed to the use of co-located (radiosonde/GCL) data in the GCL verification but not in the MAN verification. However, as noted, single soundings chosen to be co-located with radiosonde stations (see section 4c), produced only a modest improvement over the MAN set. Consequently, we conclude that while the use of co-located data sets in verification accounted for part of the superior performance of the GCL set over the MAN set, a major portion of the improvement results from the reduction of noise achieved by averaging five individual soundings.

A comparison of the reduced radiosonde networks (RR1 and RR2) with the complete radiosonde network (CRB) in Table 1 provides some insight into the influence of the density of the data network. Reducing the number of radiosonde stations by one-half yields gradient information (S1 score) somewhat better than the GCL set when the reduced radiosonde network consists of evenly spaced stations (RR1) and considerably worse when the radiosonde stations are not evenly spaced (RR2). However, replacing the missing radiosonde stations with HIRS GCL soundings produces a very marked improvement in gradient information (i.e., S1 scores) for the RS1 and RS2 sets. The addition of the satellite data to form the RS2 set produces a particularly impressive S1 improvement with a comparable improvement in the rms score.

The bias scores achieved by the various satellite data sets show a negative bias for all sets (except DST) at 850 mb, but nearly all positive values at 500 and 300 mb. This tendency indicates that the retrieved level temperatures

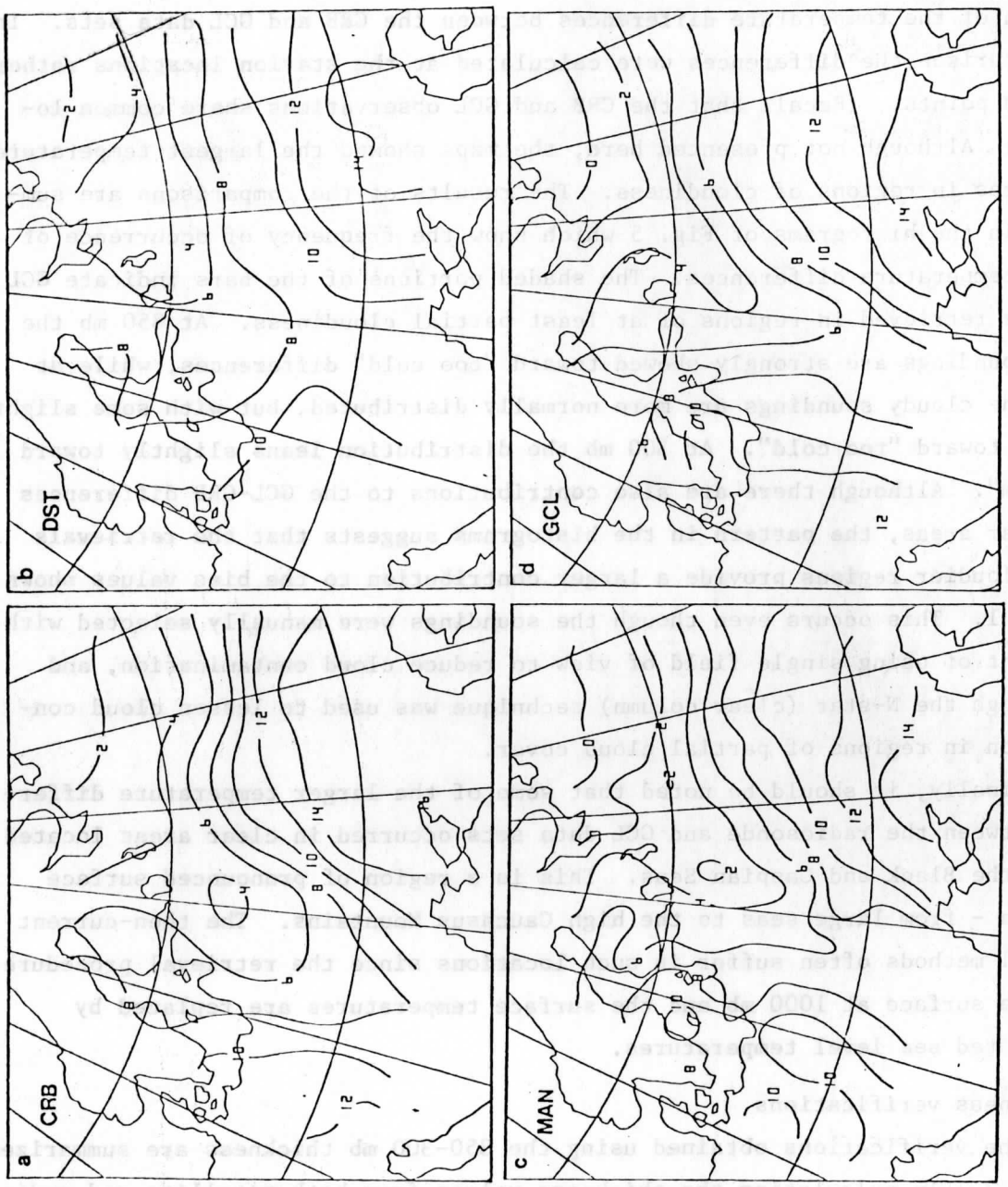

Figure 4. Temperature analyses at 850 mb at about 0000 GMT August 21, 1975: a) Complete Radiosonde network (CRB) data, b) Data System Test (DST) data, c) McIDAS, manually selected (MAN) HIRS data, d) Group Co-located (GCL) HIRS data.

at 850 mb are too cold, while at 500 and 300 mb they are too warm. This situation commonly occurs when some of the HIRS retrievals are contaminated by clouds.

To further investigate this problem, maps were prepared showing the distribution of the temperature differences between the CRB and GCL data sets. In this comparison the differences were calculated at the station locations rather than grid points. (Recall that the CRB and GCL observations share common locations.) Although not presented here, the maps showed the largest temperature differences in regions of cloudiness. The results of the comparisons are summarized in the histograms of Fig. 5 which show the frequency of occurrence of various temperature differences. The shaded portions of the bars indicate GCL soundings retrieved in regions of at least partial cloudiness. At 850 mb the cloudy soundings are strongly skewed toward "too cold" differences, while at 500 mb the cloudy soundings are more normally distributed, but with some slight tendency toward "too cold". At 300 mb the distribution leans slightly toward "too warm". Although there are also contributions to the GCL-CRB differences from clear areas, the pattern in the histograms suggests that the retrievals in the cloudier regions provide a larger contribution to the bias values shown in Table 1. This occurs even though the soundings were manually selected with the intent of using single field of view to reduce cloud contamination, and even though the N-star (clear column) technique was used to lessen cloud contamination in regions of partial cloud cover.

Finally, it should be noted that some of the larger temperature differences between the radiosonde and GCL data sets occurred in clear areas located between the Black and Caspian Seas. This is a region of pronounced surface variation - from large seas to the high Caucasus Mountains. The then-current retrieval methods often suffer in such locations since the retrieval procedure assumes a surface at 1000 mb and the surface temperatures are replaced by extrapolated sea level temperatures.

b) Thickness verifications

The verifications obtained using the 850-300 mb thickness are summarized in Table 2. In calculating the thickness values from both satellite and radiosonde data sets, only mandatory level data (850, 700, 500, 400 and 300 mb) were used in the dry hypsometric equation. Since three of these levels were examined in the previous section, it is not surprising that the trends in Tables 1 and 2 are similar. Because satellite soundings are able to describe layer mean temperatures better than level temperatures, the results shown in Table 2 are

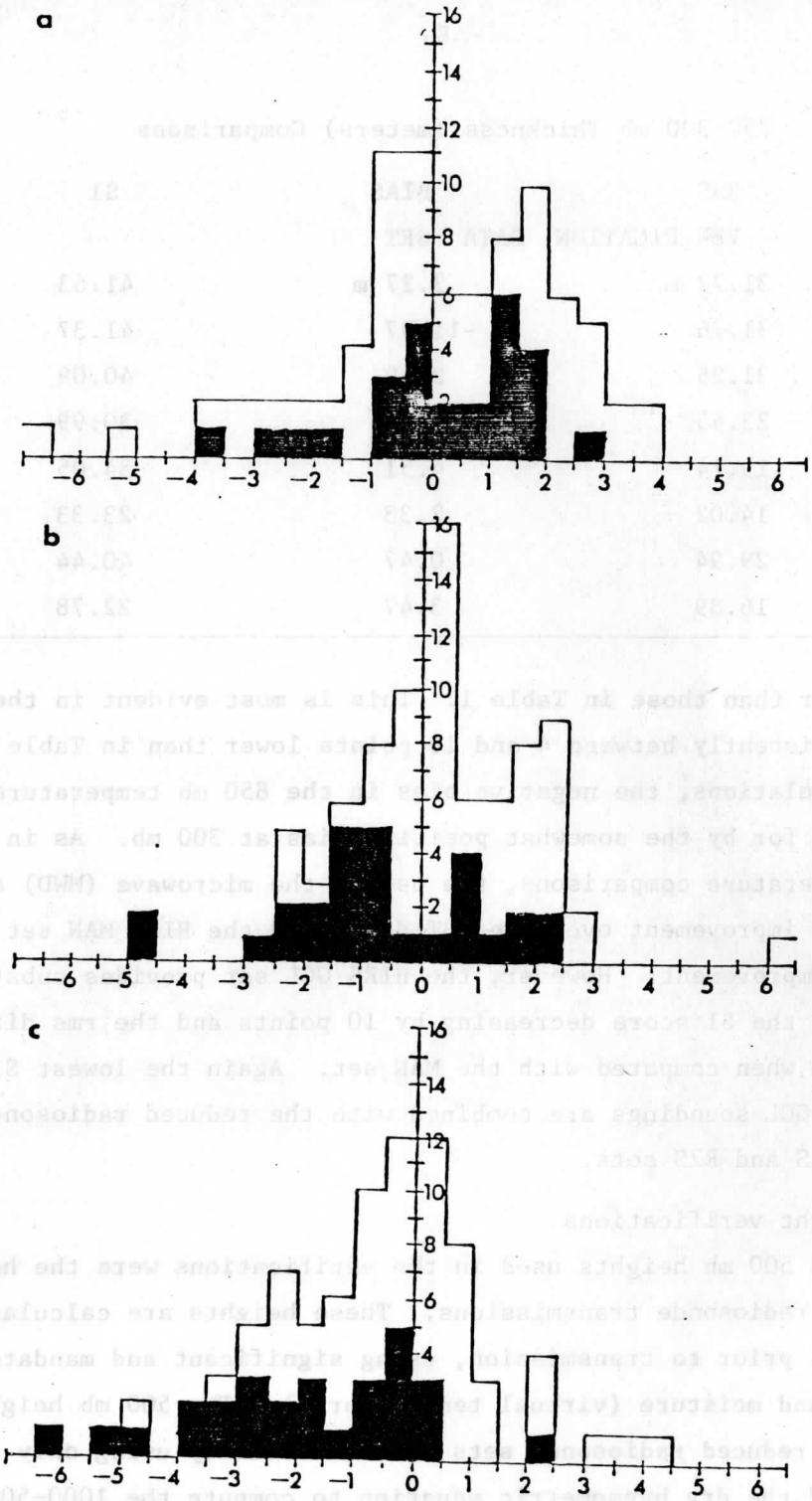

Figure 5. Histograms showing frequency of GCL and CRB temperature differences at radiosonde station locations for a) 300 mb, b) 500 mb and c) 850 mb. Shaded portions of bars indicate that the sounding was made in a relatively cloudy area. Negative values indicate that the HIRS GCL sounding was colder than the radiosonde (CRB) value.

TABLE 2

850-300 mb Thickness (meters) Comparisons

DATA	RMS	BIAS	S1
CRB	VERIFICATION	DATA SET	
DST	31.77 m	3.27 m	41.63
MWD	31.76	-11.97	41.37
MAN	31.25	2.49	40.09
GCL	23.45	4.89	30.99
RR1	19.14	4.51	34.05
RS1	14.02	2.33	23.33
RR2	29.94	0.47	40.44
RS2	16.89	3.47	22.78

somewhat better than those in Table 1. This is most evident in the S1 scores which are consistently between 4 and 10 points lower than in Table 1. In the thickness calculations, the negative bias in the 850 mb temperatures tends to be compensated for by the somewhat positive bias at 300 mb. As in the case of the level temperature comparisons, the use of the microwave (MWD) set provides essentially no improvement over the DST data, and the HIRS MAN set offers only a negligible improvement. However, the HIRS GCL set provides substantial improvement with the S1 score decreasing by 10 points and the rms difference by about 8 meters when compared with the MAN set. Again the lowest S1 scores are achieved when GCL soundings are combined with the reduced radiosonde networks to form the R1S and R2S sets.

c) 500 mb height verifications

The CRB 500 mb heights used in the verifications were the heights reported in the radiosonde transmissions. These heights are calculated at radiosonde stations prior to transmission, using significant and mandatory level temperatures and moisture (virtual temperatures). The 500 mb heights for the satellite and reduced radiosonde sets were achieved by using only mandatory level data and the dry hypsometric equation to compute the 1000-500 mb thickness. These thickness values were then added to the 1000 mb heights obtained from the CRB data to obtain the 500 mb heights. Thus this 500 mb height verification principally tests the ability of the satellite and reduced radiosonde data to describe the 1000-500 mb thickness.

Table 3a displays the 500 mb height results. In this test the microwave (MWD) set was not included. Perhaps the most striking feature of the

TABLE 3a)

500 mb Height (meters) Comparisons Using CRB
(Reduced Radiosonde Sets - Only Mandatory Level Data)

DATA CRB	RMS VERIFICATION	BIAS DATA SET	S1
DST	25.89 m	-13.80 m	37.74
MAN	33.36	-26.34	38.74
GCL	27.07	-22.74	28.41
RR1	28.00	-21.57	33.28
RS1	26.41	-23.67	22.40
RR2	29.83	-19.13	38.99
RS2	24.83	-22.13	22.52

TABLE 3b)

500 mb Height (meters) Comparisons Using CRB
(Reduced Radiosonde Sets - Mandatory and Significant Level)

DATA CRB	RMS VERIFICATION	BIAS DATA SET	S1
RR1	11.93	1.83	28.24
RS1	22.90	-14.19	24.95
RR2	22.41	- 4.02	37.20
RS2	16.41	-12.42	19.99

table is the rather uniform scores in the rms and bias scores. The negative bias is very pronounced. Only the DST data have a relatively low negative bias. However, in the S1 scores the GCL satellite data fare considerably better than the DST set, and when the GCL data are combined with RR1 and RR2 sets to form RS1 and RS2, they produce a marked improvement in the S1 scores.

Because of the large negative bias in the reduced radiosonde network data, a set of 500 mb heights were prepared in which the significant level radiosonde data were included in the RR1 and RR2 height calculations. The results in Table 3b show large improvements in the bias, and consequently also in the rms. The RR1 bias improves from -21.57 to +1.83 m, and the less uniformly spaced RR2 network from -19.13 to -4.02 m. When the satellite GCL data are included at the deleted radiosonde stations to form RS1 and RS2, the bias again becomes significantly negative, but improvements are made in the

S1 scores. This reflects a cold bias in the satellite data which was caused by the presence of nocturnal surface temperature inversions. Inversions of 5°C within 30 mb below the 900 mb level in the radiosonde soundings were common, and at one station an 11°C inversion was present. When only mandatory level radiosonde data are used, this warm layer between 1000 and 850 mb is lost. Similarly, satellite soundings with their poor vertical resolution are unable to capture this warm layer.

One additional test was conducted. Here, the 500 mb height verification data was rederived using all 96 radiosonde stations but employing only their mandatory level temperature data. Moisture was ignored.[2] This verification data set will be called the CRM set (complete set of radiosonde stations but only mandatory level data). The comparison between the CRB and CRM sets produced large rms (24.87 m) and bias (-23.76 m) values. The cold bias in the CRM set is striking; it explains more than 90% of the rms value. However, the S1 score (16.35) between the two sets is very good.

The results achieved using the CRM for verification are shown in Table 4. There is a large improvement in the rms and bias values over those shown in

TABLE 4

500 mb Height (meters) Comparisons Using CRM

DATA	RMS	BIAS	S1
CRM	VERIFICATION	DATA SET	
DST	21.63 m	9.56 m	33.70
MAN	18.69	-2.98	37.33
GCL	12.51	0.62	24.97
RR1	12.82	1.79	28.28
RS1	8.13	-0.31	17.35
RR2	23.86	4.23	35.35
RS2	8.40	1.24	17.14

Table 3. It is now the DST set which has the largest rms and bias values. The S1 scores are somewhat better in Table 4, but the major impact is in the bias and consequently in the rms. It is noteworthy that the addition of GCL satellite soundings to the RR1 and RR2 networks to form the RS1 and RS2 sets

[2] A data set based on mandatory, moist (virtual temperature) data was also obtained but it was nearly identical to the dry case.

gives excellent results. The bias and rms in the RS1 and RS2 sets are greatly reduced, and the S1 scores of 17.35 and 17.14 are essentially as good as that calculated between the two complete radiosonde networks (16.35).

Figures 6, 7 and 8 show the various 500 mb analyses over eastern Europe. In Fig. 6, are displayed the two complete radiosonde network analyses. They are quite similar except for a slightly deeper trough in the mandatory level data analysis. Figure 7 shows the DST, MAN and GCL 500 mb analyses. Note the noisier contours in the MAN (Fig. 7b) analysis compared to those in the GCL analysis (Fig. 7c). This characteristic is similar to that seen in the 850 mb temperature analyses (Fig. 4). Also note that the GCL pattern (Fig. 7c) more closely resembles the CRM pattern (Fig. 6b) than does the DST pattern (7a).

Finally, Figures 8a and 8b display the results achieved from the RR1 and RR2 data with only mandatory level data. Figures 8c and 8d incorporate HIRS GCL soundings at the missing radiosonde locations. These figures support the findings of Table 4. The addition of well screened satellite soundings to an incomplete network of mandatory level radiosonde data can produce improved analyses. Thus, satellite soundings of the quality of the GCL HIRS data appear to be compatible with mandatory level radiosonde data.

7. Conclusions

The results of this study indicate that the careful editing of satellite retrievals can produce a set of soundings camparable to mandatory level radiosonde data. The individual soundings (single spots) MAN set obtained here offered little improvement over the DST data. Single soundings co-located with 93 radiosonde locations provided some improvement over the MAN set; however, it was the averages of about five individual soundings interpolated to radiosonde locations (the GCL set) that produced soundings which were definitely superior to the DST data. While there is certainly nothing unique about choosing five soundings for the averaging, it seems clear that single soundings are likely to produce a somewhat noisy field.

Even though special editing procedures were employed to obtain the MAN and GCL sets from the Nimbus-6 HIRS data, it is apparent that there was some cloud contamination of the infrared data. This is best illustrated in Figure 5 which shows a tendency for a slightly cold bias at 850 mb and a warm bias at 300 mb. However, the relatively good performance of the GCL data set indicates that the problem was not at all severe.

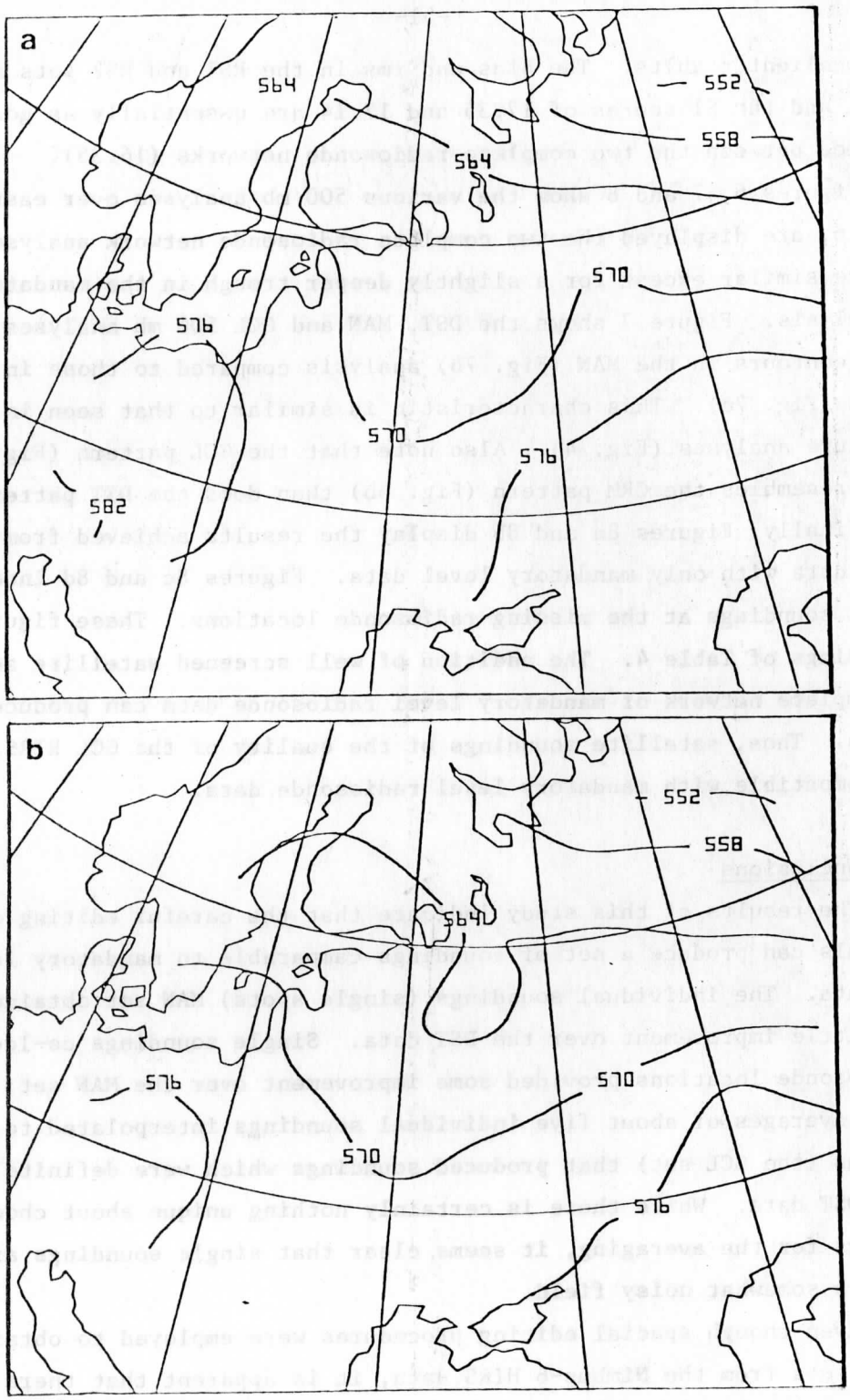

Figure 6. 500 mb height analyses for 0000 GMT August 21, 1975 based only on radiosonde data: a) Heights obtained from CRB data which includes mandatory and significant level moist data; b) Heights obtained from CRM data which uses only dry, mandatory data.

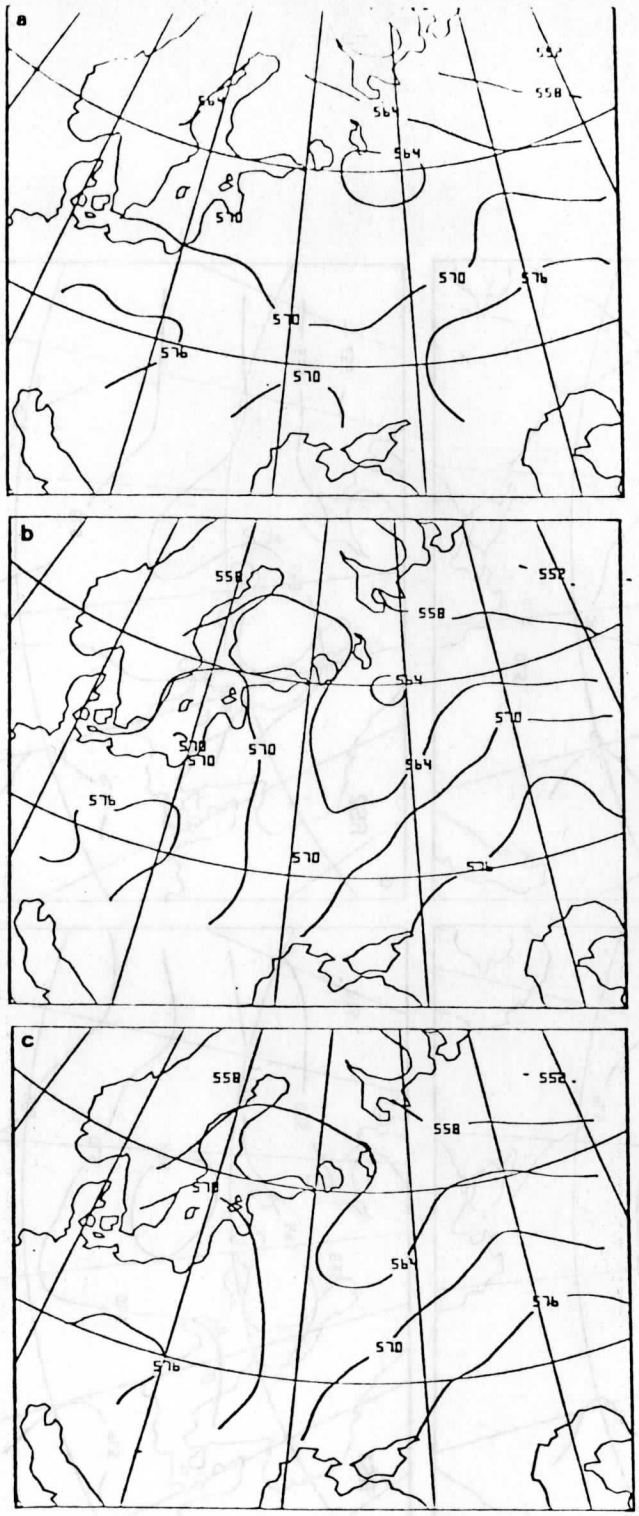

Figure 7. 500 mb height analyses based on Nimbus-6 satellite data for about 0000 GMT August 21, 1975; a) DST data set, b) HIRS manually (MAN) selected data, c) HIRS Group Co-located (GCL) data.

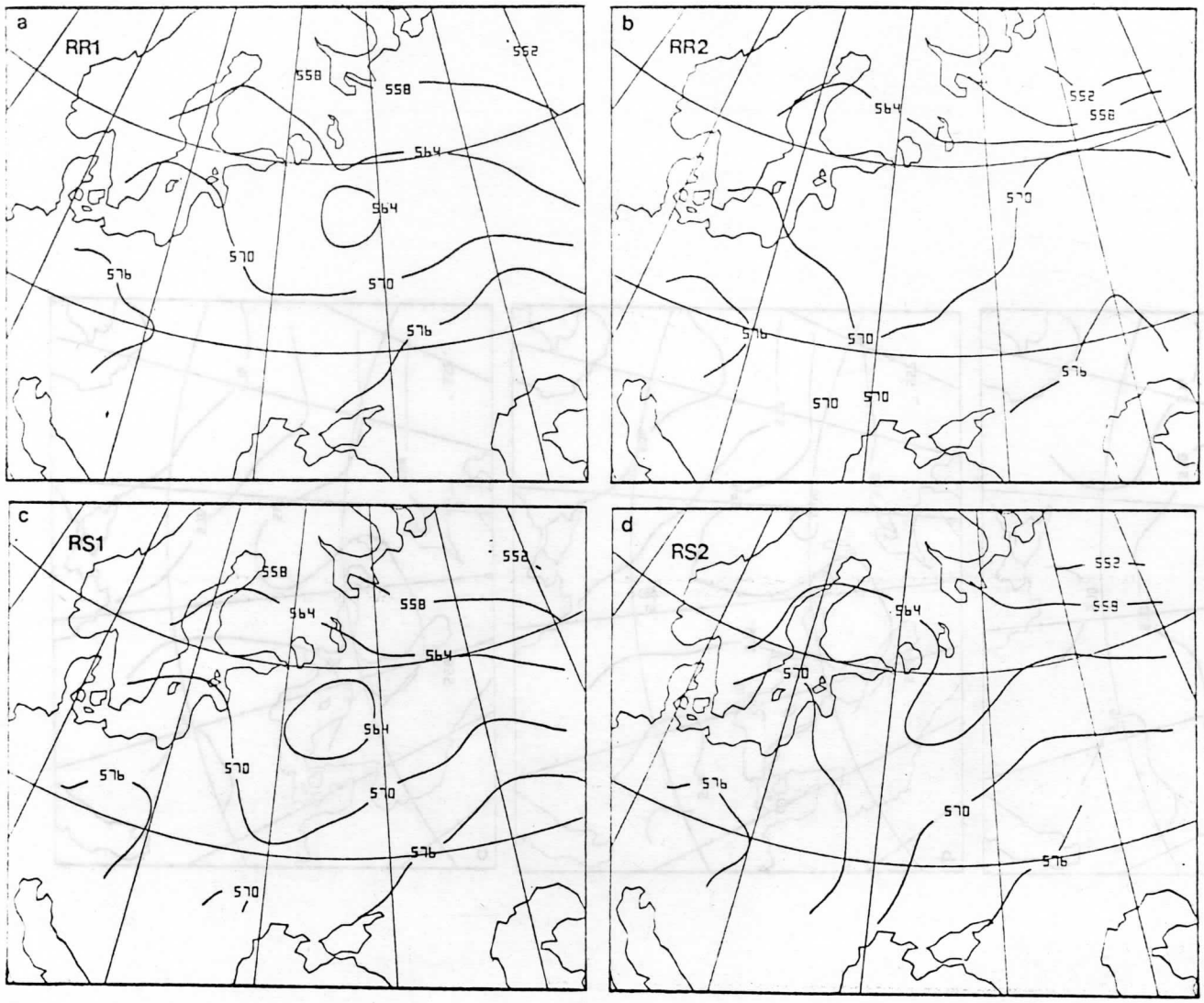

Figure 8. 500 mb height analyses obtained from: a) Reduced Radiosonde One network (RR1) data, b) Reduced Radiosonde Two network (RR2) data, c) Combination of RR1 and GCL data to form RS1 data set, d) Combination of RR2 and GCL data to form RS2 data set. See text.

The use of reduced radiosonde networks (RR1 and RR2) made it possible to examine the compatibility of satellite soundings with conventional radiosonde observations. Table 3b illustrates that even though horizontal gradients are better defined with the inclusion of satellite soundings (improved S1 scores), the lack of vertical resolution in satellite soundings produces rather large rms and bias values.

Significant nocturnal surface temperature inversions were present at the time of the observations, two to three hours past local midnight. They had a major impact as is evident in Tables 3 and 4. Since satellite soundings do not have sufficient vertical resolution to capture these inversions, the user of these data should be especially cautious with night-time soundings over land areas. The problem is made more acute if the satellite data are combined with radiosonde data consisting of both mandatory and significant level information. However, over ocean areas where nocturnal inversions are uncommon this problem is somewhat alleviated. Here exists the best opportunity for satellite soundings to fill in gaps in numerical model input. Nevertheless, further investigation is warranted into how nighttime retrievals over land can be improved.

Acknowledgments

We especially thank Dr. Christopher Hayden for his assistance both in establishing the McIDAS retrieval procedure and commenting on the manuscript. Dr. Thomas Koehler provided helpful comments during various stages of the work. Mary Hansen Bleisner, John Derber and John Buck assisted in the early portion of the work and Brian Jarvis and Kathi Marvin in the latter stage. Finally it should be noted that brisk comments by reviewer Dr. Norman Phillips strengthened the final manuscript. The research was supported by NOAA Grant numbers 04-4-158-2, NA 79AA-H-00011.

References

Ghil, M., M. Halem and R. Atlas, 1980: Time-continuous assimilation of remote-sounding data and its effect on weather forecasting. Mon. Wea. Rev., 107, 140-171.

Greaves, J.R., G. DiMego, W.L. Smith, V.E. Suomi, 1979: A special effort to provide improved sounding and cloud motion wind data for FGGE. Bull. Amer. Meteor. Soc., 60, 124-127.

Horn, L.H., R.A. Petersen and T.M. Whittaker, 1976: Intercomparisons of data derived from Nimbus-5 temperature profiles, rawinsonde observations, and initialized LFM model fields. Mon. Wea. Rev., 104, 1362-1371.

Kelly, G.A.M., G.A. Mills, W.L. Smith, 1978: Impact of Nimbus-6 temperature soundings on Australian region forecasts. Bull. Amer. Meteor. Soc., 59, 393-405.

NASA, 1975: Nimbus-6 User's Guide. Goddard Space Flight Center, Greenbelt, MD.

Petersen, R.A. and L.H. Horn, 1977: An evaluation of 500 mb height and geostrophic wind fields derived from Nimbus-6 soundings. Bull. Amer. Meteor. Soc., 58, 1195-1201.

Phillips, N.A., L.M. McMillin, A. Gruber and D.Q. Wark, 1979: An evaluation of early operational temperature soundings from TIROS-N. Bull. Amer. Meteor. Soc., 60, 1188-1197.

Phillips, N.A., 1981: Personal communication.

Smith, W.L., 1968: An improved method for calculating tropospheric temperature and moisture from satellite radiometer measurements. Mon. Wea. Rev., 96, 387-396.

Smith, W.L., C.M. Hayden, H.M. Woolf, H.B. Howell and F.W. Nagle, 1979: Satellite sounding applications to mesoscale meteorology. (COSPAR) Remote Sounding of the Atmosphere from Space, Pergamon Press Oxford, 33-47.

Smith, W.L., and H.M. Woolf, 1976: The use of eigenvectors of statistical covariance matrices for interpreting satellite sounding radiometer observations. J. Atmos. Sci., 33, 1127-1140.

Tracton, S., A. Desmarais, R. Van Haaren and R. McPherson, 1980: The impact of satellite soundings upon the National Meteorological Center's analysis and forecast system - The Data System's Test results. Mon. Wea. Rev., 108, 543-586.

Whittaker, T.M., 1976: A simplified grid interpolation scheme for use in atmospheric budget studies. M.S. thesis, Dept. of Meteor., Univ. of Wisconsin, Madison, 42 pp.

Satellite Sounding to Grid Interpolation Tests

Thomas L. Koehler

Department of Meteorology
University of Wisconsin-Madison, WI 53706

Abstract

Several methods are available for interpolating data at nonuniform observation locations to evenly spaced grid points. This study evaluates seven interpolation methods in a satellite sounding analysis application. The sensitivity of one method (optimum interpolation) to changes in its input parameters and to the presence of errors in observation is also evaluated. Analytic functions that resemble meteorological fields are used for both the observational and the verification data. Of the seven methods, optimum interpolation (OI) and two-dimensional least squares cubic fitting proved the most accurate, with OI being more economical. OI is relatively insensitive to realistic variations in the statistical parameters specified. The screening of observations to remove gross inconsistencies before analysis is necessary for any method, including OI methods designed to account for observational errors.

1. Introduction

One of the basic tasks of the satellite sounding studies done by this University of Wisconsin research group involves constructing horizontal analyses of isobaric height and temperature fields derived from satellite temperature soundings. Many objective analysis techniques have been designed, each having advantages and disadvantages. The arrangement of satellite soundings in orbital swaths with wedge-shaped data gaps between consecutive passes creates unique analysis problems. This study evaluates the accuracy of several interpolation methods when applied to this satellite sounding analysis problem. The sensitivity of one of these techniques (optimum interpolation) to changes in its input parameters is also investigated. Finally, the ability of optimum interpolation to compensate for specified sounding errors is assessed.

A sample of 271 observation locations illustrated in Figure 1 was chosen for this study from a typical August 1975 set of Nimbus-6 soundings. A subset of the National Meteorological Center's Limited-area Fine Mesh (LFM) model grid also shown in Fig. 1 serves as the analysis grid. Height data at both observation and grid point locations were specified using analytic functions based on Sanders (1971) expressions described in the appendix, which allows an exact determination of interpolation errors.

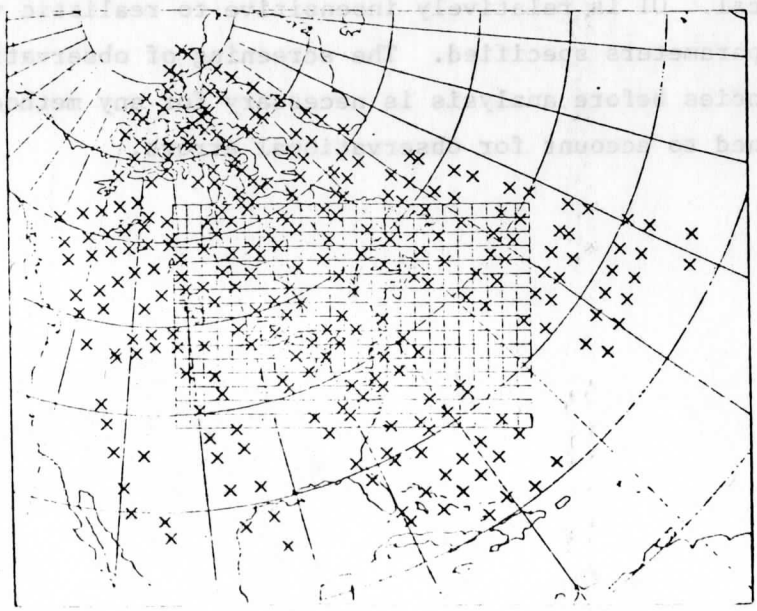

Figure 1. Observation locations used in the observation to grid interpolation tests.

Otto-Bliesner et al. (1977) note that most operational objective analysis methods perform well in regions of dense and generally uniform data coverage. However, as already mentioned, the abrupt changes in observation

density caused by the wedge-shaped spaces between satellite passes, as shown in Fig. 1, create special problems for any analysis technique.

Consider, for example, a hypothetical analysis scheme that simply assigns the mean of the five closest observations to the grid point. For the observation distribution in Figure 2, each observation would then contribute equally to the final grid point value. However, the four observations to the right of the grid point each provide less independent information than the point to the left. Although most objective analysis methods use more sophisticated weighting techniques, maximum interpolation errors for this satellite application can be expected in the wedges between satellite passes, and the analysis methods which can best handle variations in observation density should prove superior.

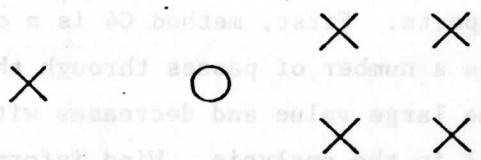

Figure 2. A hypothetical distribution of observations (X) about a grid point (O) that can cause interpolation problems.

2. Evaluation of several interpolation methods

In the first series of experiments, seven different analysis techniques are compared. These are listed in Table 1. A short description of each follows.

Table 1. Observation to grid interpolation methods.

Label	Method Description
C4	Cressman weighting technique (4 points)
C10	Cressman weighting technique (10 points)
L2	2-dimensional least squares quadratic
L3	2-dimensional least squares cubic
SD2	Shadowed inverse squared distance
BA	Barnes technique
O10	Optimum interpolation (10 points)
NO8	Optimum interpolation with normalized weights (8 points)

Methods C4 and C10 are both Cressman weighting methods which differ only in the number of points used in the analysis. In this method the

analyzed height value, h_a, is determined by a weighted sum of the closest N observations. In mathematical terms:

$$h_a = \sum_{i=1}^{N} w_i h_i \qquad (1)$$

where

$$w_i = \left(\frac{D^2-d_i^2}{D^2+d_i^2}\right) \Big/ \sum_{j=1}^{N} \left(\frac{D^2-d_j^2}{D^2+d_j^2}\right) \; ; \quad i = 1, N$$

d_i = distance in grid units from the grid point to the i^{th} observation

D = distance in grid units from the grid point to the $N+1^{th}$ observation

This method is much simpler than the Cressman (1959) analysis currently used for the LFM. While the weights are calculated in a similar manner, the two schemes differ in several other respects. First, method C4 is a one pass method. The Cressman analysis makes a number of passes through the data in which the parameter D starts at some large value and decreases with subsequent passes, to include more detail in the analysis. Wind information is also incorporated into the height analysis using the geostrophic relationship. The h's in Eq. 1 for the Cressman method are deviations from a first guess field, initially a 12 hour numerical forecast, and subsequently the previous scan's values. Thus methods C4 and C10 are much cruder than the Cressman method. However, any problems this scheme might have with varying observation density could also appear with the Cressman analysis due to the similarity of weighting methods.

The shadowed, inverse squared distance weighting scheme, SD2, was developed by Shepard (1969). The analysis value is again a weighted sum (Eq. 1). The weight determination for this method is a bit complicated. The weights start out simply as:

$$w_i = (1/d_i^2) \Big/ \sum_{j=1}^{N} (1/d_j^2) \; ; \; i=1,N \qquad (3)$$

The number of observations used in the analysis (N) varies between assigned maximum and minimum limits. An attempt is then made to compensate for interior points screening outlying points. The net effect is to ignore data from such outlying points. For more detail, refer to Shepard's article.

Methods L2 and L3 are least squares polynomial fitting methods of the following forms:

$$\text{Method L2:}\quad h_a = a_1x^2 + a_2xy + a_3y^2 + a_4x + a_5y + a_6 \tag{4}$$

$$\text{Method L3:}\quad h_a = b_1x^3 + b_2x^2y + b_3xy^2 + b_4y^3 + b_5x^2 + b_6xy + b_7y^2 + b_8x + b_9y + b_{10} \tag{5}$$

The a and b coefficients are determined through straightforward least squares techniques using the 15 observations closest to the grid point being analyzed.

The Barnes method (BA) is a two pass method. In the first pass, h_2^*, an estimate of the analyzed value at the grid point, is found as follows:

$$h_a^* = \sum_{i=1}^{N} e^{-(d_i^2/4K)} h_i \Big/ \sum_{i=1}^{N} e^{-(d_i^2/4K)} \tag{6}$$

Another pass is then made to restore wave amplitude and allow the analysis to better fit the observed data. In this scheme, N is the number of observations within a given radius of influence and K is a factor representative of the smallest resolvable feature in the data distribution. Because this method was designed to filter as well as interpolate, little or no smoothing of the final analysis is required. See Barnes (1964) and Barnes (1973) for further details.

The final two methods, 010 and NO8, are based on optimum interpolation, which was developed by Gandin (1963). Grid point values are defined as follows:

$$h_a = h_g + \sum_{i=1}^{N} w_i(h_i - h_{gi}) \tag{7}$$

where h_g = first guess values at the grid point being analyzed

h_{gi} = first guess value at observation i

The weights (w_i) in this scheme are defined through a process which minimizes the square of the analysis error over a long term sample. A system of equations with the weights as variables results from this minimization.

$$\sum_{j=1}^{N} w_j \overline{h'_i h'_j} = \overline{h'_a h'_i} \quad ; \quad i=1,N \tag{8}$$

$$h'_i = h_i - h_{gi}$$

$\overline{h'_i h'_j}$ = the first guess error covariance

The overbar indicates a long term average. Assuming the height field to have a homogeneous variance over the radius of influence for one grid point, this equation can be normalized to yield:

$$\sum_{j=1}^{N} w_j \mu_{ij} = \mu_{ai} \quad ; \quad i=1,N \tag{9}$$

where μ_{ij} is the first guess height error correlation. Equation 9 can then be solved for the weights. In method 010 data from the 10 observations closest to the grid point are used in the interpolation, and the first guess error correlation is taken from Schlatter (1975) for a persistence first guess field as follows:

$$\mu_{ij} = e^{-\beta d_{ij}} \quad ; \quad \beta = 1.24 \times 10^{-6} \text{ Km}^{-2} \tag{10}$$

First guess values at both grid and observation points were generally provided by the analytic height functions shown in the appendix with the first guess fields being displaced 5° further west than that for the observational fields.

Method NO8 is described by Gandin as optimum interpolation with normalized weights. The grid point analysis is again determined by:

$$h_a = \sum_{i=1}^{N} w_i h_i \tag{11}$$

Note that this method requires no first guess values. However the weights are still determined in a manner similar to Equation 9.

$$\sum_{J=1}^{N} w_j \mu_{ij} + \lambda = \mu_{ai} \quad ; \quad i=1,N \tag{12}$$

$$\sum_{j=1}^{N} w_j = 1$$

The variable λ and the additional equation provide a normalization of the weights necessary to preserve the mean of the analyzed field. The variable β in Equation 10 can either be prescribed by the user or defined empirically by variations in the field being analyzed and average observation spacing. The latter was used in this study for method NO8. Gandin notes that results from optimum interpolation with normalized weights will be less accurate than that from full optimum interpolation.

A comparison of the accuracy of these seven methods is presented in Table 2, in the form of bias, root mean squared and maximum errors. Exact errors were determined by subtracting the analytic value from the interpolated value at each grid point. All bias errors except those from method 010 were negative, indicating a net underestimation of the height over the area chosen. While not shown here, all maximum errors were found either in one of the two gaps between satellite passes, or in the southwest corner, a data gap within one of the passes (see Fig. 1). In general, the optimum interpolation methods, 010 and NO8, and the least squares polynomial fitting methods, L2 and L3, gave the best results. Results from the distance weighting methods were somewhat poorer. The Barnes method's performance was between these two extremes. A more detailed discussion follows.

Table 2. Height interpolation errors (m) for the different interpolation methods.

		INTERPOLATION METHODS							
	MB LEVEL	C4	C10	L2	L3	SD2	BA	010	NO8
BIAS ERRORS	1000	-.58	-155	-.18	-.10	-.32	-.22	.01	-.15
	850	-1.09	-1.56	-.18	-.05	-.62	-.43	.01	-.17
	500	-2.39	-4.12	-.16	-.06	-1.38	-.96	.00	-.21
	300	-3.09	-5.50	-.16	-.13	-1.78	-1.25	.00	-.24
ROOT MEAN SQUARED ERRORS	1000	11.3	10.2	1.8	1.2	12.3	4.4	0.8	1.2
	850	13.2	11.8	2.1	1.3	14.1	5.3	1.1	1.4
	500	20.7	18.8	3.1	1.6	21.4	8.7	2.0	2.5
	300	25.5	23.3	3.7	1.8	26.2	10.8	2.6	3.2
MAXIMUM ERRORS	1000	38.3	38.6	-9.7	-12.6	43.7	-16.8	-3.8	-15.0
	850	43.7	50.9	-11.3	12.8	51.0	-25.7	-4.7	-16.2
	500	79.0	92.4	-15.3	16.6	82.0	-52.8	-9.3	-25.3
	300	98.8	115.2	-17.5	18.6	101.5	-67.4	-11.8	-34.8

The effect of adding more observation points to the Cressman weighting technique is illustrated in comparing the results from C4 to those from C10. Because all weights used in this method are positive, the weighted sum of the observations, which provides the estimate at the grid point, must yield a value somewhere within the range of the observations used. The inclusion of data points at a greater distance from the grid point will decrease the influence of points nearer to the grid point, which usually have values closer to the actual value at the grid point, thus increasing the bias and maximum errors. However, using more observations will give smoother results as indicated by the smaller RMS errors.

Method SD2 reduces the effect of more distant observations which are screened by closer observations. This leads to smaller bias errors than those from the Cressman weighting technique. However, the higher RMS and maximum errors indicate that the inverse squared distance weighting is inadequate.

Although the Barnes method, BA, also uses simple distance-related weighting in its first pass, the second pass, which forces the analysis to better agree with the observation, allows this method to outperform the simple distance weighting methods. This is indicated by all errors for the Barnes technique being roughly half of those for the Cressman weighting method.

A comparison of the cubic and quadratic least squares fits indicates that the higher degree polynomial gives a slightly better representation, although the maximum errors for the cubic fit are slightly higher. The optimum interpolation, 010, has the smallest bias and maximum errors, while its RMS errors are slightly higher than those for the least squares cubic. The maximum errors for the normalized optimum method (NO8) are much larger than those for the optimum scheme. The errors for these last four methods (L2, L3, 010 and NO8) are all reasonable. 010 and L3 are probably the best choices from all seven methods in terms of accuracy.

Another important consideration is the computing time required for these methods. In comparing the two most accurate methods, the least squares cubic method required roughly two and one-half times as much UNIVAC 1110 computing time as the optimum interpolation, for analyses at the 10 mandatory pressure levels. The least squares analyses were made using a standard computer routine. Some duplication of effort is introduced by using this

least squares program. One matrix computed by the routine is a function only of the positions of the observations, which in this case does not change from level to level but is recomputed at every level. However, even if the time for the least squares method could be halved by more efficient programming to remove this duplication, optimum interpolation would still be more efficient. The fastest method was SD2 which used less than half the time of 010, but also gave the poorest results. Thus, for the interpolation of "perfect" data from the Nimbus-6 satellite locations, optimum interpolation appears to be the most desirable analysis method out of those tested.

3. Optimum interpolation sensitivity tests

The next set of experiments was designed to test the sensitivity of optimum interpolation to variations in certain input parameters. These involve changing one or more of the following: the number of observations in the interpolation, the first guess field, the form of the first guess error correlations, the normalization of weights, and the type of grid to observation interpolation employed. In all, eleven different tests were performed. Table 3 identifies the input parameters used in each test.

Table 3. Input parameters for the optimum interpolation tests.

Label	# of obs.	Correlation Function	First Guess	Normalized	First Guess at obs.
OP1	10	I,P	P	No	AN
OP2	10	A,P	P	No	AN
OP3	8	A,P	P	No	AN
OP4	6	A,P	P	No	AN
OP5	4	A,P	P	No	AN
OP6	10	I,C	C	No	AN
OP7	10	A,P	C	No	AN
OP8	10	I,C	P	No	AN
OP9	8	A,P	P	No	D1
OP10	8	A,P	P	No	B2
OP11	8	I,P	P	Yes	AN

I - Isotropic
A - Anisotropic
P - Persistence
C - Climatology

AN - determined analytically
D1 - interpolated from LFM grid using inverse distance weights
B2 - interpolated from LFM grid using overlapping quadratic polynomials

Three different correlation functions were applied. Two are isotropic (I) and defined by Equation 10. The values for β were taken from Schlatter (1975).

Persistence (P): $\beta = 1.24 \times 10^{-6} km^{-2}$

Climatology (C): $\beta = 0.96 \times 10^{-6} km^{-2}$

The third is anisotropic (A) and has the form

$$\mu_{ij}(\sigma,\tau) = [\cos(b_\lambda \tau) + \frac{c_\lambda}{b_\lambda} \sin(b_\lambda \tau)]e^{-c_\lambda \tau} \times \qquad (13)$$

$$[\cos(b_\phi \sigma) + \frac{c_\phi}{b_\phi} \sin(b_\phi \sigma)]e^{-c_\phi \sigma}$$

where $\sigma = r|\phi_i - \phi_j|$, $\tau = r \cos(\frac{\phi_i + \phi_j}{2})|\lambda_i - \lambda_j|$

r = radius of the earth, ϕ = latitude in radians

and λ = longitude in radians

This function was taken from Thiébaux (1977). The coefficients for a persistence first guess field are:

$$b_\phi = 1.0311 \times 10^{-3} km^{-1} , \qquad c_\phi = 0.9564 \times 10^{-3} km^{-1}$$
$$b_\lambda = 1.5906 \times 10^{-3} km^{-1} , \qquad c_\lambda = 0.3127 \times 10^{-3} km^{-1}$$

Graphs of all three correlation functions are provided in Figure 3. The choice of observations used in the analysis also depended upon the correlation function. The N observations chosen were those with the highest correlations to the grid point being analyzed. With isotropic functions this is equivalent to the N closest observations. This is not true however for the anisotropic function.

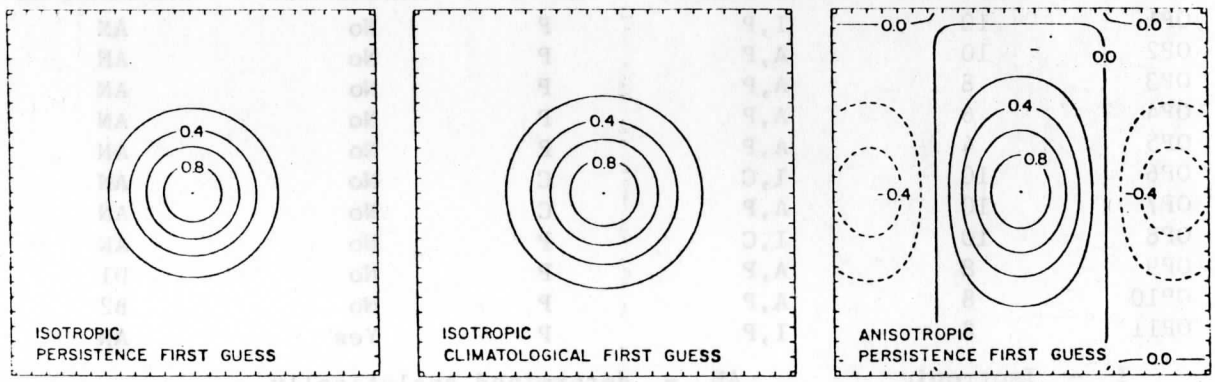

Figure 3. The three correlation functions used in the optimum interpolation tests. Tic marks are spaced every 200 km.

The persistence first guess field was again provided by the analytic functions in the appendix, with the wave displaced 5° longitude further west than the observational wave. Parameters for the climatological first guess field are also given in the appendix, which provided a smaller amplitude wave of longer wavelength. First guess values at observation points were either

determined analytically (AN), or interpolated from the LFM grid using either an inverse distance weighting method (D1) or overlapping quadratic polynomials (B2), two methods evaluated in Koehler (1977). The normalization of weights was performed in the manner described in Equations 12.

The error statistics for these various methods are presented in Table 4. Method OP1 is identical to method O10 in the previous discussion, and differs from method OP2 only in the form of the correlation function. The anisotropic method (OP2) gives slightly lower RMS and maximum errors but has slightly higher bias errors.

Table 4. Height interpolation errors (m) for the variations of optimum interpolation.

		INTERPOLATION METHODS										
	MB LEVEL	OP1	OP2	OP3	OP4	OP5	OP6	OP7	OP8	OP9	OP10	OP11
BIAS ERRORS	1000	.01	-.06	-.06	-.09	.08	-.03	.09	-.01	-.15	-.10	-.08
	850	.01	-.05	-.07	-.10	.07	-.03	.11	-.01	-.12	-.11	-.09
	500	.00	-.04	-.08	-.13	.04	-.01	.17	-.01	-.03	-.12	-.12
	300	.00	-.04	-.09	-.15	.03	.00	.20	-.01	.02	-.12	-.13
ROOT MEAN SQUARED ERRORS	1000	0.8	0.7	0.9	1.0	1.8	1.0	1.6	0.5	2.6	0.9	0.9
	850	1.1	0.7	0.9	1.0	2.0	1.0	1.6	0.6	3.0	0.9	0.9
	500	2.0	1.1	1.1	1.2	3.3	1.0	1.8	1.0	5.0	1.2	2.2
	300	2.6	1.4	1.4	1.4	4.3	1.0	1.9	1.2	6.4	1.4	2.8
MAXIMUM ERRORS	1000	-3.8	-4.1	-3.8	4.1	9.2	-4.4	10.5	2.1	-12.8	-3.7	-5.5
	850	-4.7	-4.9	-4.2	3.9	-13.4	4.3	10.9	2.7	-16.6	-4.7	-6.4
	500	-9.3	-7.1	-7.1	5.0	-23.7	4.3	12.0	-4.7	-26.3	-7.5	8.8
	300	-11.8	-8.2	-8.6	-8.8	-29.3	4.5	12.5	-5.8	-31.5	-9.1	10.8

The effect of decreasing the number of observations used in the interpolation is illustrated in the results from methods OP2 through OP5, where the number per grid point is decreased in steps of two from ten to four. Only small error increases can be detected in decreasing the observations from ten to six. A threshold is crossed somewhere between six and four points, where the bias changes sign and the maximum errors at 850, 500 and 300 mb more than triple. The computing time needed to solve the simultaneous weight equations for optimum interpolation is proportional to N^3, where N is the number of observations used in the interpolation. Considerable savings can then be made

by using fewer points. Care must be taken not to degrade the analysis by using too few points.

Method OP6 employed climatology for both the first guess fields and the correlation function. The RMS and maximum errors for this method show little variation, a quite surprising result for the height field whose variance increases with altitude. The results for methods OP7 and OP8 show the effect that mixing first guess fields and correlation functions of different types has upon the final analysis. The best results of any of the methods were from OP8, a mixture of persistence first guess fields and a climatological correlation curve. The inverse mixture, OP7, exhibited relatively poor bias and maximum errors. The better results for the schemes using weights determined from the climatological correlation function may be related to the relatively long wavelength (60° longitude) of the feature these analysis methods are trying to describe. (See Figure A1.) At shorter wavelengths, other combinations may perform better.

Methods OP9 and OP10 are presented to emphasize the need for an accurate interpolation of first guess values to observation points. A relatively poor (D1) and an accurate (B2) grid to observation interpolation methods were employed in OP9 and OP10 respectively. The standard for this experiment is OP3. This method used the same input parameters, but with "perfect" first guess values at the observations. Method OP10 (B2) has only slightly higher errors than OP3. However, the RMS and maximum errors for OP9 (D1) are roughly four times as large as those for OP3. Thus, the analyses are degraded to the degree expected from Koehler (1977). The maximum errors are even larger than expected for the inverse distance weighting method (D1).

The last method, OP11, is the method used in studies such as Koehler (1979) with real sounding data. It is only presented here to give some idea of its performance with respect to other optimum interpolation methods. This method uses eight observations per grid point. Normalization of the interpolation weights was incorporated to solve a problem encountered in the wedge-shaped data void regions. The sum of weights in these regions show a high frequency oscillation, as shown in Figure 4 for method OP2. Such an oscillation could lead to noise in the final analysis. Also, since the observations with the highest correlations to a given grid point were used in its analysis, the sharp variation of the anisotropic correlation function in the

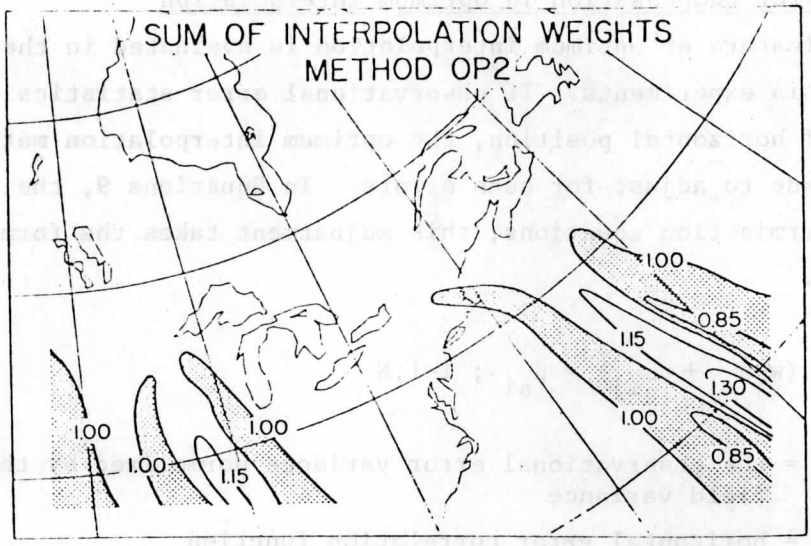

Figure 4. Sum of the interpolation weights for a now-normalized optimum interpolation method. The sums in shaded regions are less than one.

east-west direction caused some problem in the selection of observations for the interpolation. A return to the isotropic correlation function remedied this selection problem.

While normalization is included, OP11 is not identical to method NO8. This is because deviations from the first guess field are still used in the interpolation, and the β value is prescribed from Schlatter (1975). As might be expected this method gives slightly higher error values than OP3, its anisotropic, non-normalized equivalent, and lower error values than those found from NO8.

The error levels for most of the different optimum interpolation tests with perfect data are quite small. Only when too few observations are included (OP5) or a poor interpolation is employed to obtain first guess values at observations (OP9), do the errors reach levels that cause concern. At 300 mb where the range in the height field is over 900 m, maximum errors of less than 12 m (~ 1%) are quite acceptable. To be able to say with certainty that one of these variations of optimum interpolation is superior to any of the others would require more exhaustive tests with analytical waves of different wavelength and shape, and differing positions within the observational sample.

4. Tests for error compensation in optimum interpolation

Another feature of optimum interpolation is evaluated in the final series of analysis experiments. If observational error statistics are known as a function of horizontal position, the optimum interpolation method can, in theory, be made to adjust for such errors. In Equations 9, the interpolation weight determination equations, this adjustment takes the form of an additional term.

$$\sum_{j=1}^{N} (w_j \mu_{ij} + \eta \rho_{ij}) = \mu_{ai} \quad ; \; i=1,N \tag{14}$$

where η = the observational error variance normalized by the field variance

ρ_{ij} = horizontal error correlation function

This form of the equation ignores any correlation between data and error values. Note that for truly random errors, ρ_{ij} will equal 1 for i equal to j, and zero otherwise.

In the tests presented here, errors typical of satellite soundings are added to the analytic observations, and error statistics for Nimbus-6 sounding during DST-6 are incorporated into the interpolation weight determination scheme. This should present an estimate of the effectiveness of this error compensation within the interpolation method.

Two kinds of error were added to simulate satellite sounding errors. First, satellite temperatures reported at a given level are more representative of a mean temperature for some finite layer of the atmosphere, rather than the temperature at a given pressure. Smith (1978) determined the pressure layers centered about 5 mandatory levels which give radiosonde layer mean temperatures best correlated to satellite "level" temperatures during DST-5. The depths of these 5 pressure layers are plotted at 0's in Figure 5. At 500 mb, for example, the depth is 500 mb. This means that layer mean temperatures calculated between 750 and 250 mb yield the highest correlation to 500 mb temperature retrievals from Nimbus-6 during DST-5. A linear interpolation was made between these points to estimate the pressure interval used to calculate the layer mean temperatures at the 21 pressure levels between 1000 and 100 mb where Nimbus-6 temperature data are normally available. This pressure interval was artificially forced to zero at 1000 and 100 mb. The

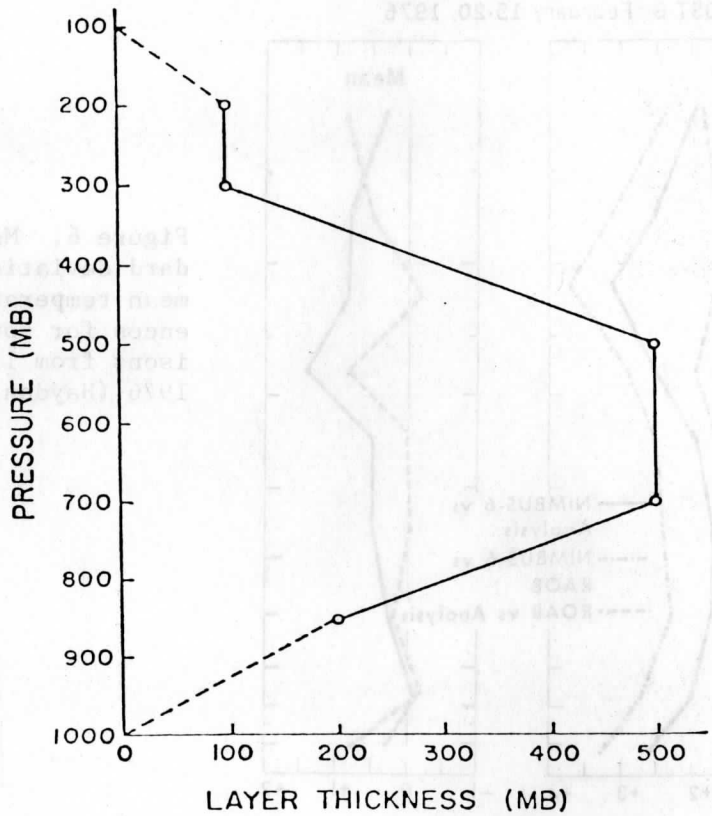

Figure 5. Thickness of a layer centered about a given pressure level for which the layer mean temperature determined from radiosonde measurements was most highly correlated with the satellite-derived temperature reported at that level (Smith, 1978).

vertically averaged temperatures were incorporated to simulate the correlated nature of satellite temperature errors. Heights at mandatory levels were then computed using a finite difference form of the hypsometric equation and these temperatures.

A random error was then added to the mandatory level height data in the following manner. Standard deviations of Nimbus-6 layer mean temperature errors between mandatory level pressures were taken from the Nimbus-6 vs. analysis graph in Figure 6, from Hayden (1977). (The mean error curve was not used because the vertical averaging described earlier provides this type of error.) A random number generator provided the layer mean temperature errors at each observation, which were then translated into height errors.

Three interpolation tests were performed with this error data. The experiments are labelled and described in Table 5. The results from these experiments are presented in Table 6 with results from method OP2, which used

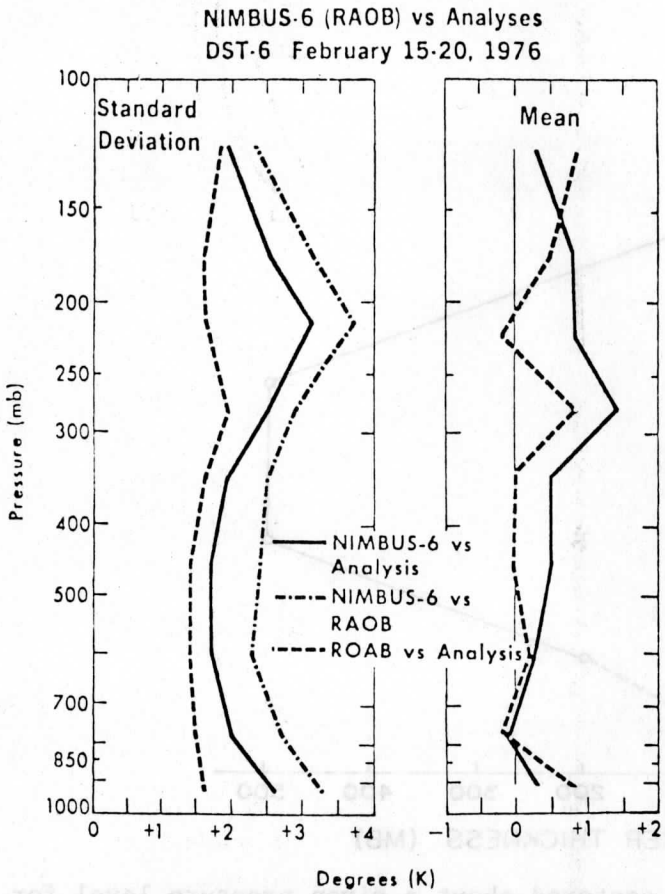

Figure 6. Means and standard deviations of layer mean temperature differences for sounding comparisons from 15-20 February 1976 (Hayden, 1977).

Table 5.

Label	Method Description
VA	Vertically averaged data with perfect weights (from method OP2)
EP	Vertically averaged data with random errors and perfect weights
EE	Vertically averaged data with random errors and error compensated weights

perfect data and weights determined from Equation C9, repeated as a standard. In the results for VA, the vertically averaged data, note the bias errors increasing in magnitude with altitude. The analytic temperature expressions use a specified constant positive lapse rate (no inversions or isothermal layers). Thus layer mean temperatures calculated using these analytic expressions will continually underestimate the level temperature, as indicated by the negative bias. This underestimate becomes larger as the depth of the

Table 6. Height interpolation errors (m) for the tests with imperfect data. Results for method OP2 with perfect data are included for comparison.

		METHODS			
	MB LEVEL	OP2	VA	EP	EE
BIAS ERRORS	1000	-.06	-0.1	-0.1	0.2
	850	-.05	-0.3	-1.0	-0.8
	500	-.04	-29.6	-29.8	-28.8
	300	-.04	-55.2	-53.6	-52.3
ROOT MEAN SQUARED ERRORS	1000	0.6	0.6	0.6	2.0
	850	0.7	0.8	14.0	10.1
	500	1.1	30.8	39.2	34.6
	300	1.4	57.4	63.7	58.3
MAXIMUM ERRORS	1000	-4.1	-4.1	-4.1	-4.6
	850	-4.9	-5.4	-40.1	-34.7
	500	-7.1	-54.8	-115.5	-95.7
	300	-8.3	-101.4	-163.7	-133.9

layer over which the mean temperature is calculated increases. As illustrated in Figure 5, these layers are much deeper above 850 mb than below. Thus, the level temperature underestimates are larger above 850 mb than below. In computing the heights, these level temperatures are integrated vertically. The larger temperature underestimates combined with integration over a much deeper layer (850 mb to 500 mb layer compared to the 1000 mb to 850 mb layer) help to explain the abrupt change in height bias errors between 850 mb and 500 mb. The next test (EP) uses the vertically averaged data to which random errors have been added. As expected, analysis errors above 850 mb show a substantial increase over those from the VA test. The values at 1000 mb did not change because no errors were added at this level, and the interpolation weights were the same as for methods OP2 and VA.

In the final test (EE) weights were determined with the additional term in Equation 14. The spatial error correlation function was defined by a least squares fit to data taken from Figure 7, also from Hayden (1977). A curve of the form:

$$\rho_{ij} = \alpha e^{-\beta d_{ij}} + \gamma \qquad (15)$$

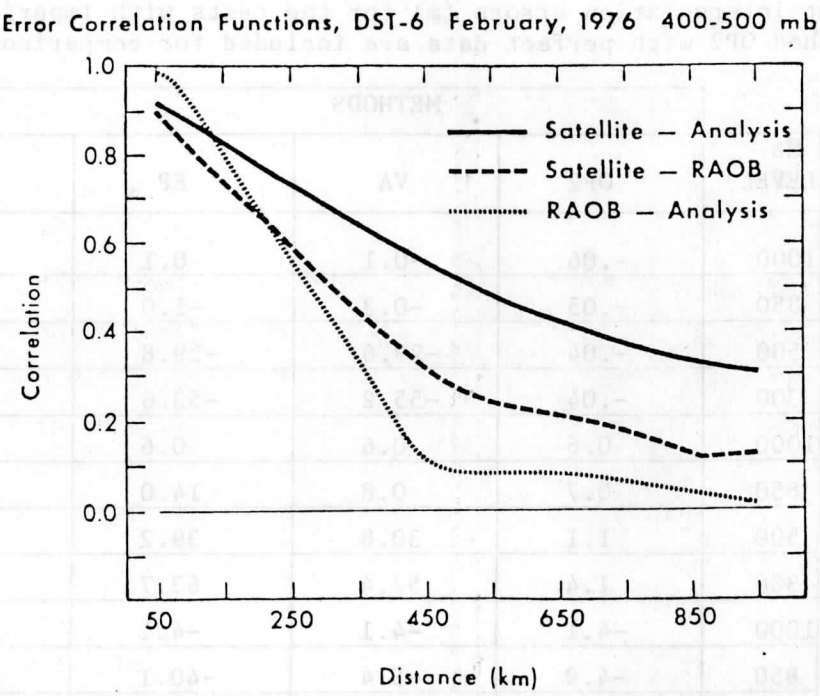

Figure 7. Satellite sounding error correlation functions in the 400-500 mb layer for the same period as Fig. 6 (also from Hayden, 1977).

was fit to data from the Satellite vs. Analysis graph in this figure. The resulting coefficients were $\alpha = .6974$, $\beta = 4.07 \times 10^{-6} km^{-2}$ and $\gamma = .3026$. The α term was modified to insure that $\rho_{ij} = 1$ at $d_{ij} = 0$. The form for this curve is similar to that used by Bergman and Bonner (1976) to simulate Nimbus-5 satellite temperature errors.

The normalized error variance, η, was determined as follows. Standard deviations were taken from Figure 6 for both Nimbus-6 vs. Analysis and RAOB vs. Analysis. These values were then weighted by the appropriate pressure differences to find representative layer mean temperature standard deviations for both RAOB ($\bar{\sigma}_{RAOB}$) and satellite ($\bar{\sigma}_{SAT}$) errors. Using a value for η of .04 for radiosonde height data, as suggested in Schlatter (1975) for a persistence first guess field, η for the DST-6 Nimbus-6 height data was then estimated by:

$$\eta_{SAT} = \frac{\bar{\sigma}^{-2}_{SAT}}{\bar{\sigma}^{2}_{RAOB}} \eta_{RAOB} \simeq 0.0725 \qquad (16)$$

The results for test EE in Table 5 indicate the effect that including these observational error statistics in the determination of optimum interpolation weights has upon the final analysis. Some minor improvement is shown at and above 850 mb. The 500 mb analyses for methods VA, EP, and EE are shown in Figure 8. The analysis from method OP2 is also presented as a perfect data standard. The analysis with error weights (EE) is smoother than that for the perfect weights (EP). However, this smoothing is not enough. The bias error introduced artificially by using layer mean temperatures was virtually untouched by the correlated observational error information incorporated into the analysis. While more accurate observational error statistics may improve the analysis results, the effects of errors in individual observations may not be fully removed as indicated in the above figure.

5. Conclusions

Optimum interpolation and least squares cubic fits performed best in these satellite sounding analysis tests. Optimum interpolation costs less than least squares fitting, making it the more desirable method. Simple distance weighting schemes did not perform well in the gaps between satellite passes.

Varying the input parameters in optimum interpolation methods has only minor inpact on the error statistics. Using too few observations in the interpolation, or a poor grid to observation interpolation method in the transfer of first guess values from a grid to the sounding locations can degrade the optimum interpolation results. Large fluctuations in the sum of the interpolation weights are encountered in the data gap regions when using the anisotropic correlation function.

Both bias and random errors were added to the analytic observations in the final series of interpolation tests to simulate satellite sounding errors. The incorporation of error statistics into the optimum interpolation method yielded only a modest reduction of the random error components, and little reduction of the bias errors. Manual or automated screening of data before it enters an optimum interpolation analysis system will still be required to remove gross errors or inconsistencies.

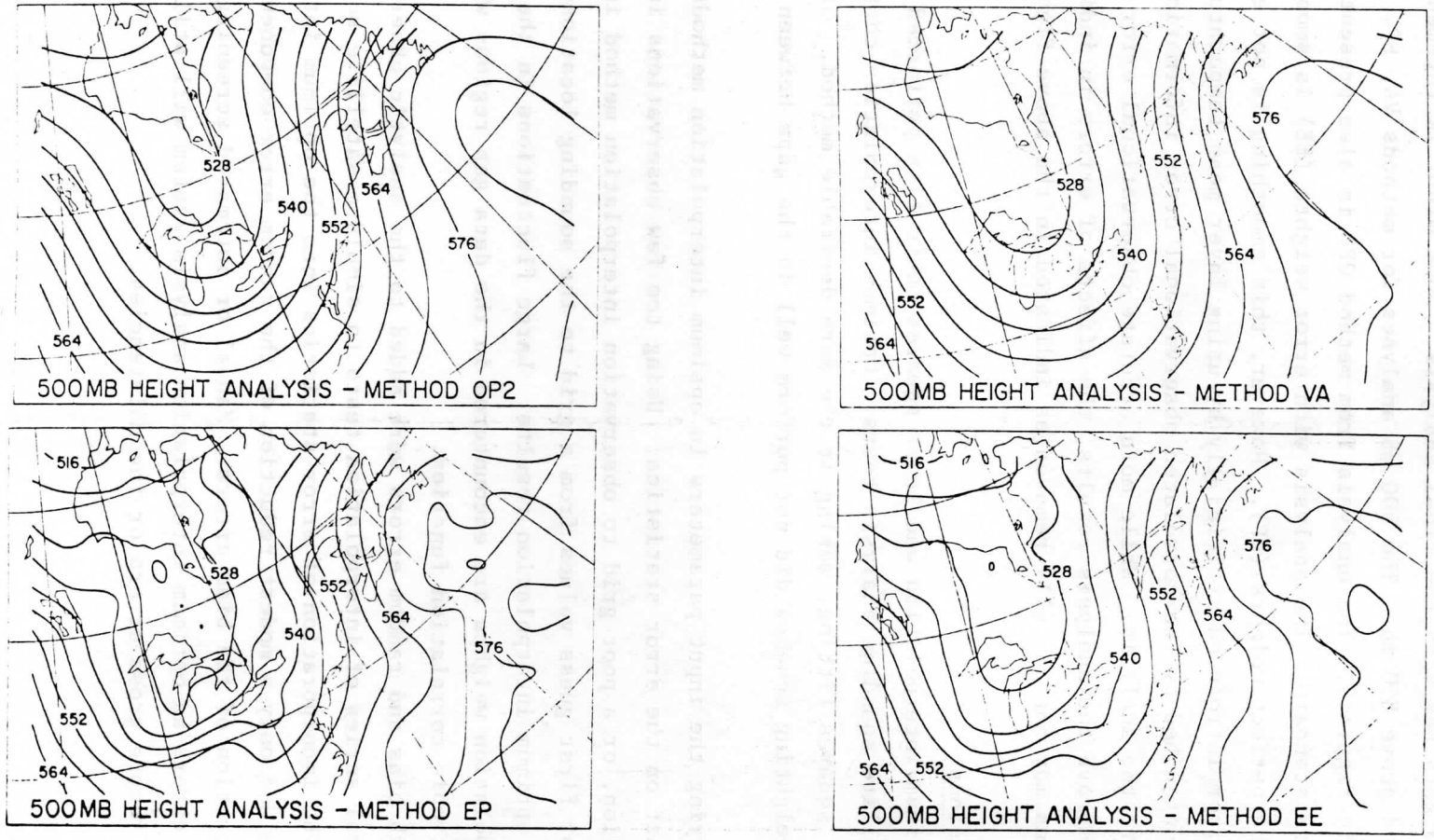

Figure 8. Height analyses (dam) for four of the analysis tests which evaluate the effects of measurement errors. (See text.)

Appendix - An analytic representation of temperature and height fields

Meaningful tests of analysis methods require data sets with known values at both grid and observation points. The 3-dimensional analytic functions used to derive height and temperature values for the analysis experiments discussed in this paper are presented in this appendix. A structural model of atmospheric variables applied by Sanders (1971) provided the basis for the functional forms used here.

The expressions for temperature and height are as follows:

$$T(\lambda,\phi,p) = T_m(1000)\left(\frac{p}{1000}\right)^{R\gamma/g} - (1-\alpha)\ln\frac{1000}{p}$$

$$\left\{\frac{ar}{\sin\phi_o}(\cos\phi_o - \cos\phi) + \hat{T}\cos\left[\frac{2\pi}{L_\lambda}(\lambda_o - \lambda)\right]G(\phi)\right\} \qquad \text{(A1)}$$

$$Z(\lambda,\phi,p) = \hat{Z}\cos\left[\frac{2\pi}{L_\lambda}(\lambda_o - \lambda + \Delta\lambda)\right]G'(\phi) + \bar{Z} +$$

$$\frac{T_m(1000)}{\gamma}\left[1 - \left(\frac{p}{1000}\right)^{R\gamma/g}\right] - \frac{R}{g}\left[\ln\frac{1000}{p} - \frac{\alpha}{2}\left(\ln\frac{1000}{p}\right)^2\right]$$

$$\left\{\frac{ar}{\sin\phi_o}(\cos\phi_o - \cos\phi) + \hat{T}\cos\left[\frac{2\pi}{L_\lambda}(\lambda_o - \lambda)\right]G(\phi)\right\} \qquad \text{(A2)}$$

where

λ = longitude (positive west) in radians

ϕ = latitude in radians

p = pressure in millibars

L_λ = east-west wavelength of the disturbance in radians longitude

$\Delta\lambda$ = a parameter which controls the phase lag of the 1000 mb height relative to the 1000 mb temperature (radians longitude)

λ_o = reference longitude

ϕ_o = reference latitude

$T_m(1000)$ = mean temperature at 1000 mb

$\hat{Z}$ = amplitude of the 1000 mb height disturbance

$\bar{Z}$ = mean 1000 mb height

$\hat{T}$ = amplitude of the 1000 mb temperature disturbance

r = radius of the earth (6371 km)

a = magnitude of the north-south temperature gradient

α = a parameter that determines the pressure of the troposphere

γ = lapse rate of the mean temperature profile

and R/g = ratio between the gas constant for dry air and gravity.

The $G(\phi)$ and $G'(\phi)$ functions control the north-south variations in the 1000 mb temperature and height disturbances, respectively. They are modeled as follows:

$$G(\phi) = b[\frac{18}{\pi}(\phi-\phi_o)]^6 + c[\frac{18}{\pi}(\phi-\phi_o)]^4 + d[\frac{18}{\pi}(\phi-\phi_o)]^2 + e \qquad \text{(A3)}$$

$$G'(\phi) = \frac{2}{\sin\phi_o}\frac{18^4}{\pi^2}\{[-36\frac{18^4}{\pi^4}(\phi-\phi_o)^5 + (60b\frac{18^4}{\pi^4} - 2c\frac{18^2}{\pi^2})(\phi-\phi_o)^3 +$$

$$[15b\frac{18^4}{\pi^4}(\phi-\phi_o)^4 + (-180b\frac{18^4}{\pi^4} + 6c\frac{18^2}{\pi^2})(\phi-\phi_o)^2 +$$

$$(360b\frac{18^4}{\pi^4} - 12c\frac{18^2}{\pi^2} + d)]\sin\phi -$$

$$(360b\frac{18^4}{\pi^4} - 12c\frac{18^2}{\pi^2} + d)\sin\phi_o\} + e \qquad \text{(A4)}$$

Figure A1 illustrates the height and temperature fields used for the observation and verification values in the analysis experiments. They were generated using the following values:

$T_m(1000) = 278K$ $\qquad$ $\Delta\lambda = 18°$

$\hat{T} = 10K$ $\qquad$ $L_\lambda = 60°$

$\hat{Z} = 150$ m, $\bar{Z} = 90$ m $\qquad$ $\lambda_o = 90°$, $\phi_o = 45°$

$\frac{R\gamma}{g} = .0953$ $\qquad$ $\alpha = .621$ (trop at 200 mb)

$a = 0.9 \times 10^{-5}$ °C/m

$b = -1/60$, $c = 11/60$, $d = -2/3$, $e = 1$

The persistence first guess fields were defined using the same parameters, except λ_o was set equal to 95°. The climatological first guess fields were constructed by changing the following parameters:

$\hat{Z} = 60$ m $\qquad$ $L_\lambda = 90°$

$\hat{T} = 5K$ $\qquad$ $\lambda_o = 100°$

The fields calculated from these functions are not able to fully represent true atmospheric fields. However, they do resemble meteorological fields,

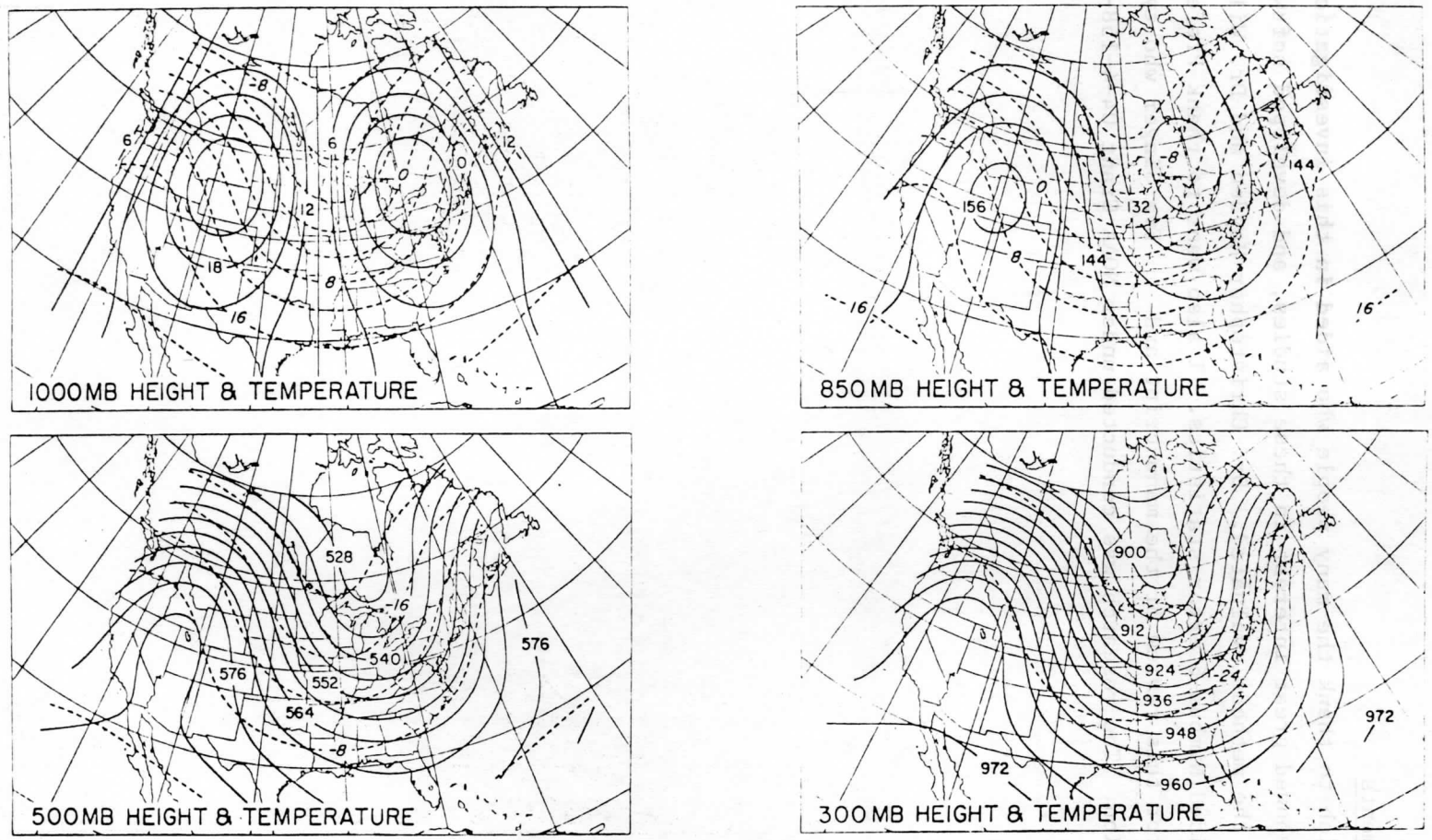

Figure A1. Sample analytic fields at selected isobaric levels. Height contours (dam) are solid and isotherms (°C) are dashed.

and exhibit enough nonlinearity to adequately identify the problems and merits of the interpolation methods being tested.

Acknowledgments

I wish to thank the many people who aided in this investigation. Tom Whittaker showed great interest in these studies, and developed software for several of the methods evaluated. Dr. Christopher Hayden and Dr. William Smith provided Nimbus-6 error statistics. I also want to thank Professor Lyle Horn for this review of the manuscript and Eva Singer who typed the final version. The research was conducted under NOAA Grant 04-4-158-2.

References

Barnes, S.L., 1964: A technique for maximizing details in numerical weather map analysis. J. Appl. Meteor., 3, 369-409.

Barnes, S.L., 1973: Mesoscale objective map analysis using weighted time-series observations. NOAA Tech. Memo. ERL NSSL-62.

Bergman, K.H. and W.D. Bonner, 1976: Analysis error as a function of observation density for satellite temperature soundings with spatially correlated errors. Mon. Wea. Rev., 104, 1308-1316.

Cressman, G., 1959: An operational objective analysis system. Mon. Wea. Rev., 87, 367-374.

Gandin, L.S., 1963: Objective Analysis of Meteorological Fields. Gidrometeorologich eskoe Izdatel'svto, Leningrad. Translated from Russian, Israel Program for Scientific Translations, Jerusalem, 1965, 242 pp.

Hayden, C.M., 1977: A summary of Nimbus-6 temperature retrieval accuracy statistics for DST-5 and DST-6. Third NASA Weather and Climate Program Science Review. NASA Conference Publication 2029, Goddard Space Flight Center, Greenbelt, MD.

Koehler, T.L., 1977: A test of seven methods which perform grid to observation interpolations. Meteorological Applications of Satellite Indirect Soundings II, Project Report, NOAA Grant 04-4-158-2, Dept. of Meteorology, University of Wisconsin, Madison.

Koehler, T.L., 1979: A case study of height and temperature analyses derived from Nimbus-6 satellite soundings on a fine mesh model grid. Ph.D. Thesis, University of Wisconsin, Madison, 186 pp.

Otto-Bliesner, B., D.P. Baumhefner, T.W. Schlatter, and R. Bleck, 1977: A comparison of several meteorological analysis schemes over a data rich region. Mon. Wea. Rev., 105, 1083-1091.

Sanders, F., 1971: Analytic solutions of the nonlinear omega and vorticity equations for a structurally simple model of disturbance in the baroclinic westerlies. Mon. Wea. Rev., 99, 393-407.

Schlatter, T.W., 1975: Some experiments with a multivariate statistical objective analysis scheme. Mon. Wea. Rev., 103, 246-257.

Smith, W.L., 1978: Personal communication, University of Wisconsin, Madison.

Thiébaux, H.J., 1977: Extending estimation accuracy with anisotropic interpolations. Mon. Wea. Rev., 105, 691-699.